Discovery and characterization of novel imidazopyridine derivative CHEQ-2 as a potent CDC25 inhibitor and promising anticancer drug candidate

ARTICLE *in* EUROPEAN JOURNAL OF MEDICINAL CHEMISTRY · MAY 2014

Impact Factor: 3.45 · DOI: 10.1016/j.ejmech.2014.05.063 · Source: PubMed

7 AUTHORS, INCLUDING:

Peng Zhan
Shandong University
134 PUBLICATIONS **1,194** CITATIONS
SEE PROFILE

Xinyong Liu
Shandong University
144 PUBLICATIONS **1,342** CITATIONS
SEE PROFILE

European Journal of Medicinal Chemistry 82 (2014) 293–307

Contents lists available at ScienceDirect

European Journal of Medicinal Chemistry

journal homepage: http://www.elsevier.com/locate/ejmech

Original article

Discovery and characterization of novel imidazopyridine derivative CHEQ-2 as a potent CDC25 inhibitor and promising anticancer drug candidate

Yu'ning Song [a], Xiaoqian Lin [a], Dongwei Kang [b], Xiao Li [b], Peng Zhan [b, *], Xinyong Liu [b, *], Qingzhu Zhang [a, *]

[a] Department of Pharmacology, Key Laboratory of Chemical Biology (Ministry of Education), School of Pharmaceutical Sciences, Shandong University, 44 West Culture Road, 250012, Jinan, Shandong, PR China
[b] Department of Medicinal Chemistry, Key Laboratory of Chemical Biology (Ministry of Education), School of Pharmaceutical Sciences, Shandong University, 44 West Culture Road, 250012, Jinan, Shandong, PR China

ARTICLE INFO

Article history:
Received 18 March 2014
Received in revised form
6 May 2014
Accepted 26 May 2014
Available online 27 May 2014

Keywords:
CDC25 inhibitor
Anticancer agents
Cell cycle arrest
Apoptosis
Reactive oxygen species

ABSTRACT

Cell division cycle (CDC) 25 proteins are key phosphatases regulating cell cycle transition and proliferation *via* the interactions with CDK/Cyclin complexes. Overexpression of CDC25 proteins is frequently observed in cancer and is related to aggressiveness, high-grade tumors and poor prognosis. Thus, inhibiting CDC25 activity in cancer treatment appears a good therapeutic strategy. In this article, refinement of the initial hit XDW-1 by synthesis and screening of a focused compound library led to the identification of a novel set of imidazopyridine derivatives as potent CDC25 inhibitors. Among them, the most potent molecule was CHEQ-2, which could efficiently inhibit the activities of CDC25A/B enzymes as well as the proliferation of various different types of cancer cell lines *in vitro* assay. Moreover, CHEQ-2 triggered S-phase cell cycle arrest in MCF-7, HepG2 and HT-29 cell lines, accompanied by generation of ROS, mitochondrial dysfunction and apoptosis. Besides, oral administration of CHEQ-2 (10 mg/kg) significantly inhibited xenografted human liver tumor growth in nude mice, while demonstrated extremely low toxicity (LD_{50} > 2000 mg/kg). These findings make CHEQ-2 a good starting point for further investigation and structure modification.

1. Introduction

As well known, different types of cancers may have different pathogenesis and show diverse clinical symptoms, but one of the most prominent features shared in cancer cells is deregulated growth [1,2]. The uncontrolled proliferation is mostly attributed to cell cycle deregulation [3,4]. Cell cycle is a tightly controlled procedure, which needs a delicate signaling network to determine the proper progression [4,5]. Cyclin-dependent kinases (CDKs) are foremost cell cycle regulators that phosphorylate and activate downstream players like retinoblastoma (Rb) protein to promote cell cycle progression [6]. The cell division cycle 25 (CDC25) family of proteins are highly conserved dual specificity phosphatases that could activate CDKs, which in turn regulate progression through the cell division cycle.

CDC25 dual phosphatase family can be found in all eukaryotic organisms except plants. In mammalian cells, it has three members: CDC25A, CDC25B, and CDC25C [7]. CDC25A acts on the control of G1-to-S and G2-to-S transitions in cell cycle whereas CDC25B and CDC25C are mainly responsible for regulating the progression at the G2-to-M transition. CDC25B is proposed to be responsible for the initial activation of CDK1–Cyclin B at the centrosome during the G2–M transition [8–10], which is then followed by a complete activation of CDK1–Cyclin B complexes by CDC25C in the nucleus at the onset of mitosis [11]. Owing to such an important contribution to the cell cycle regulation, CDC25 phosphatases have been considered to be involved in oncogenic transformations and human cancers. CDC25A and CDC25B overexpression are frequently found in many cancers, such as breast cancer, colorectal cancer, hepatocellular carcinoma, non-Hodgkin lymphoma etc., and are often associated with high-grade tumors and poor prognosis. Therefore, the inhibition of CDC25 phosphatases may represent a novel

* Corresponding authors. School of Pharmaceutical Sciences, Shandong University, 44 West Culture Road, 250012, Jinan, Shandong, PR China.
E-mail addresses: zhanpeng1982@163.com (P. Zhan), xinyonglab@163.com (X. Liu), zhangqzh@sdu.edu.cn (Q. Zhang).

http://dx.doi.org/10.1016/j.ejmech.2014.05.063
0223-5234/

approach for the development of anticancer therapeutics, although more details about the involvement of CDC25A and CDC25B overexpression in tumorigenesis remain to be clarified.

Many compounds with CDC25 phosphatase inhibitory activities are currently being developed. The existing structural types include quinonoids, phosphate surrogates, or electrophilic derivatives [12]. Starting from the structure of vitamin K published in 1993 as a potent CDC25 inhibitor [13], numerous compounds were derived from a *para*-quinonoid structure. And many other quinonoid derivatives were able to inhibit CDC25 activity and tumor cell proliferation. The most potent quinonoid-based compounds identified so far are active on xenografted tumor models. To date, there is no suitable inhibitor for further drug development, and thus innovative compounds are required.

Recently, 1,2,4-triazole derivative XDW-1 (compound **4**, Scheme 1) was identified as a novel inhibitor of CDC25 phosphatase *via* a virtual screening approach [14]. This compound was structurally original unlike the existing *para*-quinonoid structure and exhibited a significant potency in micromolar range, providing a new scaffold for further development as anticancer drugs by structure–activity relationships (SARs) studies or in-depth druggability investigations.

To obtain the structural insight into the inhibitory actions and to underline the potential of this new type of CDC25 phosphatase inhibitor, herein, optimization of the initial hit XDW-1 by synthesis and preliminary screening of a focused compound library with led to the identification of a set of novel imidazopyridine derivatives as potent CDC25 inhibitors. Further *in vitro* and *in vivo* investigations led to the identification of compound CHEQ-2 as a promising anticancer drug candidate with remarkable antiproliferative effects.

2. Chemistry

The lead compound 2-(4-(4-chlorophenyl)-5-p-tolyl-4H-1,2,4-triazol-3-ylthio)-1-(3,4-dihydroxyphenyl)ethanone (**4**, XDW-1) was obtained by the alkylation reaction of 4-(4-chlorophenyl)-5-p-tolyl-4H-1,2,4-triazole-3-thiol (**3**) (CAS No. 451501-95-4) [15] with 2-chloro-1-(3,4-dihydroxyphenyl)ethanone (**2**) in the presence of K_2CO_3 in an easy, rapid and profitable way (Scheme 1). Similarly, the newly designed compounds (CHEQ-2 (**9a**), CHEQ-1 (**9b**), CHEQ-3 (**13a**), CHEQ-4 (**13b**), CHEQ-5 (**16a**) and CHEQ-6 (**16b**)) were synthesized by alkylation reaction of intermediates 1-mesityl-1H-imidazo[4,5-c]pyridine-2-thiol (**8a**) or 3-mesityl-3H-imidazo[4,5-b]pyridine-2-thiol (**8b**) with 2-chloro-1-(3,4-dihydroxyphenyl)ethanone (**2**), N-(2-aminophenyl)-2-chloroacetamide (**12**), or *N*-(2-hydroxyphenyl)-2-chloroacetamide (**15**) in good yields (Schemes 2 and 3). The key intermediates **8a** and **8b** were synthesized according to the reported literature with minor modification [16]. Both analytical and spectral data of all the newly synthesized compounds are in full agreement with the proposed structures.

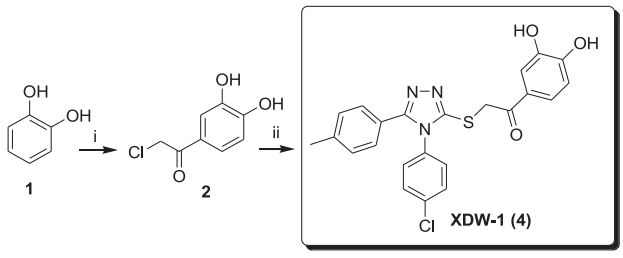

Scheme 1. Reagents and conditions: (i) 2-chloroacetyl chloride, $AlCl_3$, $ClCH_2CH_2Cl$; (ii) 4-(4-chlorophenyl)-5-p-tolyl-4H-1,2,4-triazole-3-thiol (**3**), K_2CO_3, acetone.

3. Results and discussions

3.1. Evaluation of CHEQ-1–CHEQ-6 in vitro CDC25 inhibition and cell growth suppression

The six newly synthesized compounds (*CHEQ-1–CHEQ-6*) were evaluated for their inhibitory effects against the recombinant full length CDC25A and CDC25B, and the growth of colon carcinoma HT-29 cells and hepatoma HepG2 cells. The results, expressed as IC_{50} values are summarized in Table 1 together with those of lead compound XDW-1 and a classic positive compound vitamin K3 (VK3) as the references.

As listed in Table 1, the six imidazopyridine derivatives showed notable activity against CDC25A/B with IC_{50} values ranged from 0.3 to 30 μM. Compound CHEQ-1 (IC_{50} = 0.30 μM), CHEQ-2 (IC_{50} = 0.39 μM), and CHEQ-6 (IC_{50} = 0.64 μM) showed comparable inhibitory potential with two reference compound VK3 (IC_{50} = 0.80 μM) and XDW-1 (IC_{50} = 0.28 μM) against CDC25A. Regarding the CDC25B inhibition, the majority of them showed comparable activity with two reference compounds (IC_{50} values in the range of 1.26–6.67 μM), except for CHEQ-6 (IC_{50} = 16.61 μM). Especially, compound CHEQ-2 was approximately 3-fold and 2-fold more effective against CDC25B compared to XDW-1 and VK3, respectively. Interestingly, compared with CDC25B, CDC25A demonstrated more sensitive profiles towards nearly all the tested compounds including two reference ones (except for CHEQ-5). It is not hard to find that the position of nitrogen atom in imidazopyridine and the nature of the substituent groups linked to "$-SCH_2CO-$" essentially influenced the inhibitory activity and selectivity of CDC25A/B.

After analyzing their biochemical actions on CDC25A/B, we then focused our attention on the evaluation of their ability to block proliferation of two human tumor cells in culture. Except for CHEQ-4 (IC_{50} > 100 μM in HT-29) and CHEQ-6 (IC_{50} > 100 μM in HepG2), other compounds displayed equivalent or more potent antiproliferative activities in HT-29 and HepG2 cell lines. Notably, CHEQ-2 and CHEQ-5 were the most potent inhibitors of cell proliferation, especially for HepG2 with IC_{50} values of 11.25 and 11.77 μM, respectively.

All in all, of all the tested compounds, CHEQ-2 exhibited the most potent inhibition against CDC25A/B as well as cell growth among all the compounds. Comparing with XDW-1 and VK3, CHEQ-2 showed comparable inhibition potential on enzymes (both CDC25A and B) and much stronger suppression on cell growth. These preliminary results demonstrated that the isosteric replacement of imidazopyridine for 1,2,4-triazole core ring in XDW-1 was gratifying and afforded a set of potent imidazopyridines with CDC25A/B and tumor inhibiting activity *in vitro*.

Further, the inhibitory effects of CHEQ-2 on a mass variety of different tumor cells, e.g. colon carcinoma, mammary carcinoma, hepatoma, microglioma, etc., were investigated. Encouragingly, as highlighted in Table 2, CHEQ-2 led to a decreased viability in these different tumor cells. And most of the IC_{50} values were below 20 μM. In contrast, XDW-1 and VK3 showed much weaker inhibition on most of the tested cell lines. The IC_{50} values were much higher, approximately two or three times of CHEQ-2 in most cases. However, The IC_{50} value of CHEQ-2 in neuroblastoma cells SH-SY5Y and drug-resistant mammary carcinoma MCF-7/A cells was a little higher, approximately 35 μM, demonstrating that these cells were less sensitive to CHEQ-2. Normal hepatocyte L-02 cells and rat primary cultured neurocytes were also found less sensitive to CHEQ-2 according to our results, indicating CHEQ-2 had relatively low toxicity toward these normal cells.

According to these results, CHEQ-2, as the most promising molecule was selected and further investigated, both *in vitro* and

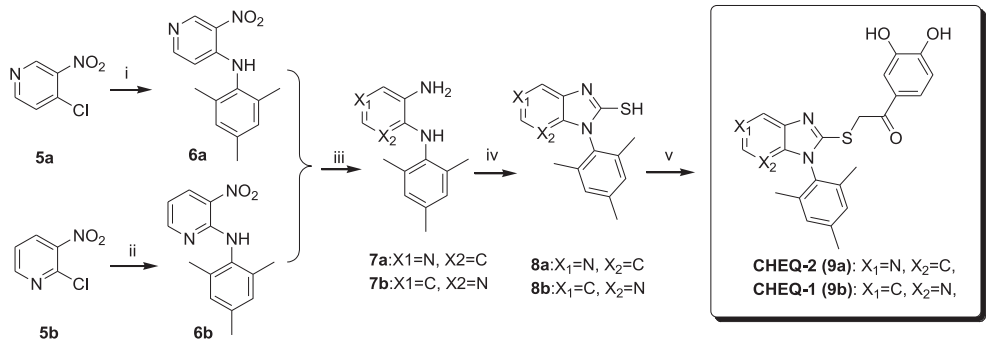

Scheme 2. Reagents and conditions: (i) 2,4,6-trimethylbenzenamine, $NaHCO_3$, EtOH, reflux; (ii) 2,4,6-trimethylbenzenamine, KF, 120 °C; (iii) H_2, Pd/C; (iv) $NaHCO_3$, EtOH, H_2O, $CH_3CH_2OCS_2K$, reflux, acidification; (v) 2-chloro-1-(3,4-dihydroxyphenyl)ethanone (**2**), K_2CO_3, acetone.

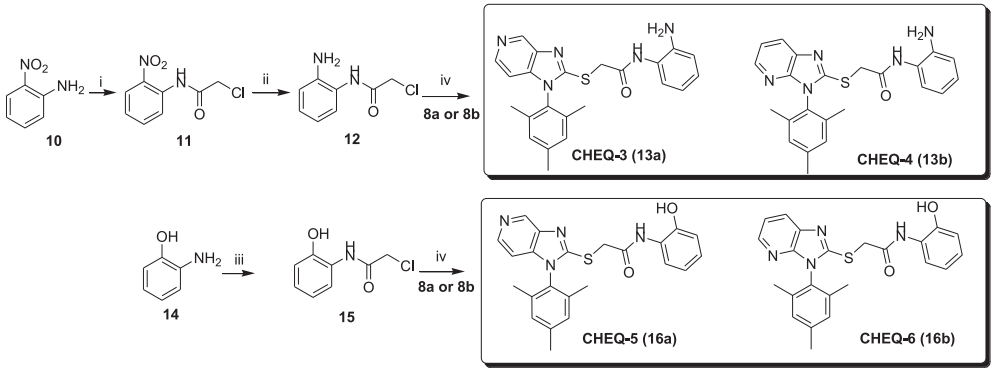

Scheme 3. Reagents and conditions: (i) 2-chloroacetyl chloride, DCM, Et_3N; (ii) Fe, NH_4Cl, AcOH, DMF, H_2O; (iii) 2-chloroacetyl chloride, chloroacetic acid, 1,2-dichloroethane; (iv) K_2CO_3, DMF.

in vivo inhibitory potential effects. As described above, CDC25 proteins reported to be overexpressed in many tumor tissues, especially in the samples from patients with breast, colorectal and hepatocellular cancers etc [17]. Therefore, three different CDC25 overexpression human tumor cell lines MCF-7 of breast cancer, HepG2 of hepatocellular cancer and HT-29 of colorectal cancer were applied in our research. In consistent with previous result, cell viability study displayed that CHEQ-2 displayed much stronger inhibitory potential than VK3 and XDW-1 at nearly all doses against MCF-7, HepG2 and HT-29 cell lines (As shown in Fig. 1).

3.2. CHEQ-2 induced S-phase cell cycle arrest by inhibiting CDC25 expression

Cells were treated with different doses of CHEQ-2 (7.5, 15, 30 μM) for 12, 24 and 48 h. The distribution in different phases of the cell cycle is illustrated in Fig. 2. The results demonstrated CHEQ-2 treatment could trigger significant reduction of G0/G1 phase cells in all three different tumor cell lines MCF-7 (Fig. 2A), HepG2 (Fig. 2C) and HT-29 (Fig. 2E). And this reduction was accompanied by an apparent increase in the proportion of cells in the S phase in concentration-dependent manner. And the maximum increases of S-phase cell fraction reached 40.0% (MCF-7), 38.1% (HepG2) and 27.7% (HT-29) respectively. However, the changes of G2/M cells were varied by different cell lines, which can be explained by tiny distinguishment existed in cell-type specific molecular mechanisms of CHEQ-2.

Our choice of the cell cycle related proteins tested in this study is partly related to the importance of their role in the control of the cell cycle. Regardless of the initial insult, the net result is an inhibition of CDK–Cyclin complexes in order to stop cell-cycle progression. It has been illustrated that CDC25 mainly activates the CDK2–Cyclin E and CDK2–Cyclin A complexes during the G1–S transition [18–20], but also has a role in the G2–M transition [21,22] by activating CDK1–Cyclin B complexes. Moreover, it has been proved that CDK2–Cyclin A complex is also necessary for cells progression through the S phase [23], and CDK2 is the primary downstream substrate of CDC25A which activates CDK2/Cyclin A complex [24]. Cyclin B is also indispensable in the control of the onset of mitosis. As remarkable S-phase cell cycle arrest was found in CHEQ-2 treated cells, we speculated that CHEQ-2 could affect these cell cycle proteins, including CDK2, Cyclin A, B and E, as well as CDC25A and B. In consistent with our speculation, it was showed that CHEQ-2 not only suppressed the expression of CDC25A and B, but also inhibited the expression of CDK2, Cyclin A, B and E (See Fig. 2B, D, F), which mediated the S-phase cell cycle arrest. However, the expression of Cyclin A and B didn't show any reduction in CHEQ-2 treated HT-29 cells (Fig. 2F), which could help to explain the relative insensitivity of HT-29 (IC_{50} value was nearly twice that of MCF-7 and HepG2 cells).

3.3. CHEQ-2 induced apoptosis cell death

The induction of apoptosis by CHEQ-2 was first examined by Hoechst staining under fluorescence microscopy. The changes in cell nuclear morphology were shown in Fig. 3A. After treatment with CHEQ-2 for 48 h, cells of all three cell lines showed bright fluorescent nuclei blebbing and DNA fragmentation, comparing

Table 1
In vitro IC_{50} values (μM) of CHEQ1–6 against CDC25 (A and B) and two cell lines (HT-29 and HepG2) in MTT assay.

Compounds	IC_{50}(μM)			
	Enzymes		Cell lines	
	CDC25A	CDC25B	HT-29	HepG2
CHEQ-1	0.30	4.30	28.87	21.93
CHEQ-2	0.39	1.26	24.20	11.25
CHEQ-3	2.58	4.91	23.76	22.05
CHEQ-4	3.64	3.84	>100	99.44
CHEQ-5	29.03	6.75	23.26	11.77
CHEQ-6	0.64	16.61	39.67	>100
XDW-1	0.28	3.48	37.26	21.06
VK3	0.80	2.58	31.30	42.11

Table 2
IC_{50} values (μM) of VK3, XDW-1 and CHEQ-2 against different kinds of tumor cell lines in MTT assay.

Tumor	Cell line	IC_{50}(μM)		
		VK3	XDW-1	CHEQ-2
Colon carcinoma	SW620	23.79	20.61	11.40
	SW480	47.51	30.43	15.47
	HCT-116	29.35	23.59	15.47
Mammary carcinoma	MCF-7	22.76	28.84	14.35
Hepatoma	H-7402	47.88	64.19	27.17
Microglioma	BV2	4.79	5.82	7.98
Neuroblastoma	SH-SY5Y	26.13	>100	34.12
Drug-resistant mammary carcinoma	MCF-7/A	39.32	69.36	37.17
Human normal fetal hepatocyte cell line	L-02	19.11	46.81	35.29
Rat primary cultured neurocytes	Primary cells	30.26	>100	>1000

with non-treated control. An increase of apoptotic cells accompanied by a drop of cell density could be observed in a dose-dependent manner. These changes are in accordance with the characteristics of apoptosis cell death.

CHEQ-2-induced apoptosis was also confirmed by flow cytometric analysis of MCF-7, HepG2 and HT-29 cells stained with annexin V and PI (Fig. 3B). The results demonstrated that CHEQ-2 caused a dose-dependent increase in both early and late stage of apoptosis in all three cell lines, and the apoptosis rate increased to 49.5% (MCF-7), 45.7% (HepG2), and 52.8% (HT-29).

Evaluation of apoptosis protein confirmed that CHEQ-2 treatment could cause obvious apoptosis associated with down-regulation of Bcl-2 expression, and elevate Bax protein levels in MCF-7, HepG2 and HT-29 cells (Fig. 3C). It was also found that CHEQ-2 dramatically induced activation of caspase 3 and PARP. It is thought that Bcl-2 and Bax are involved in the regulation of mitochondrial outer membrane permeabilization and subsequent activation of caspase 3 and PARP [25–27].

3.4. CHEQ-2 induced generation of reactive oxygen species and loss of mitochondrial membrane potential

ROS is associated with many crucial factors in apoptosis signal pathways, and abnormally high concentration of ROS is an important cause of cell apoptosis. Therefore, we examined whether there is more ROS production upon CHEQ-2 administration. To this end, we performed DCFH-DA-based fluorescence detection by both fluorescence microscopy and flow cytometry in MCF-7, HepG2 and HT-29 cells. The results showed that CHEQ-2 treatment elevated ROS levels in all three cell lines in a dose-dependent manner (As shown in Fig. 4A).

Moreover, oxidative stress is always closely linked with mitochondrial dysfunction. Mitochondrial membrane potential is the hallmark of the status of mitochondrial membrane, and a mitochondrial potential sensor JC-1 was used to determine the mitochondria function. It forms J-aggregates in intact mitochondria that result in emission of red/orange fluorescence, whereas it forms monomers upon the mitochondrial membrane depolarization that emit green fluorescence [28]. As shown in Fig. 4B, CHEQ-2 treatment resulted in a dose-dependent loss of mitochondrial potential in all three cell lines, as evidenced by the shift of fluorescence. And 30 μM of CHEQ-2 caused an increase (31.1% (MCF-7), 67.6% (HepG2) and 29.1% (HT-29)) of cells with green fluorescence (See Fig. 4C), indicating that CHEQ-2 treatments led to reduction of mitochondrial membrane potential and dysfunction of mitochondria.

3.5. NAC blocked the CHEQ-2-induced ROS generation and mitochondrial damage, and attenuated the CHEQ-2-induced cell growth inhibition

The antioxidant NAC was employed to determine the contribution of ROS in the anti-cancer effects of CHEQ-2. As shown in Fig. 5A, cellular ROS level in MCF-7, HepG2, and HT-29 cells was significantly increased after the treatment of 30 μM CHEQ-2 for 48 h. As anticipated, 5 mM NAC significantly suppressed CHEQ-2-induced ROS generation in all three cell lines. Moreover, NAC could also abrogate the loss of mitochondrial membrane potential in all three cell lines. As shown in Fig. 5B, NAC treatment attenuated CHEQ-2 induced elevation of percentages of cells with green fluorescence. Meanwhile, it was noteworthy that CHEQ-2-mediated inhibition on MCF-7, HepG2 and HT-29 cell viability was also compromised by the treatment of 5 mM NAC (Fig. 5C), further suggesting the contribution of CHEQ-2-induced ROS accumulation in its anti-cancer properties.

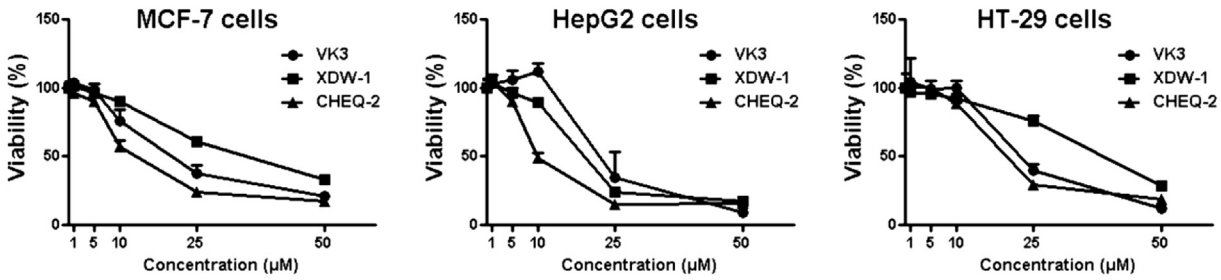

Fig. 1. Evaluation of cell viability of MCF-7, HepG2 and HT-29 cells treated with DMSO, VK3, XDW-1 or CHEQ-2 1, 5, 10, 25, 50 μM for 48 h. The data were expressed as mean ± SD ($n = 5$).

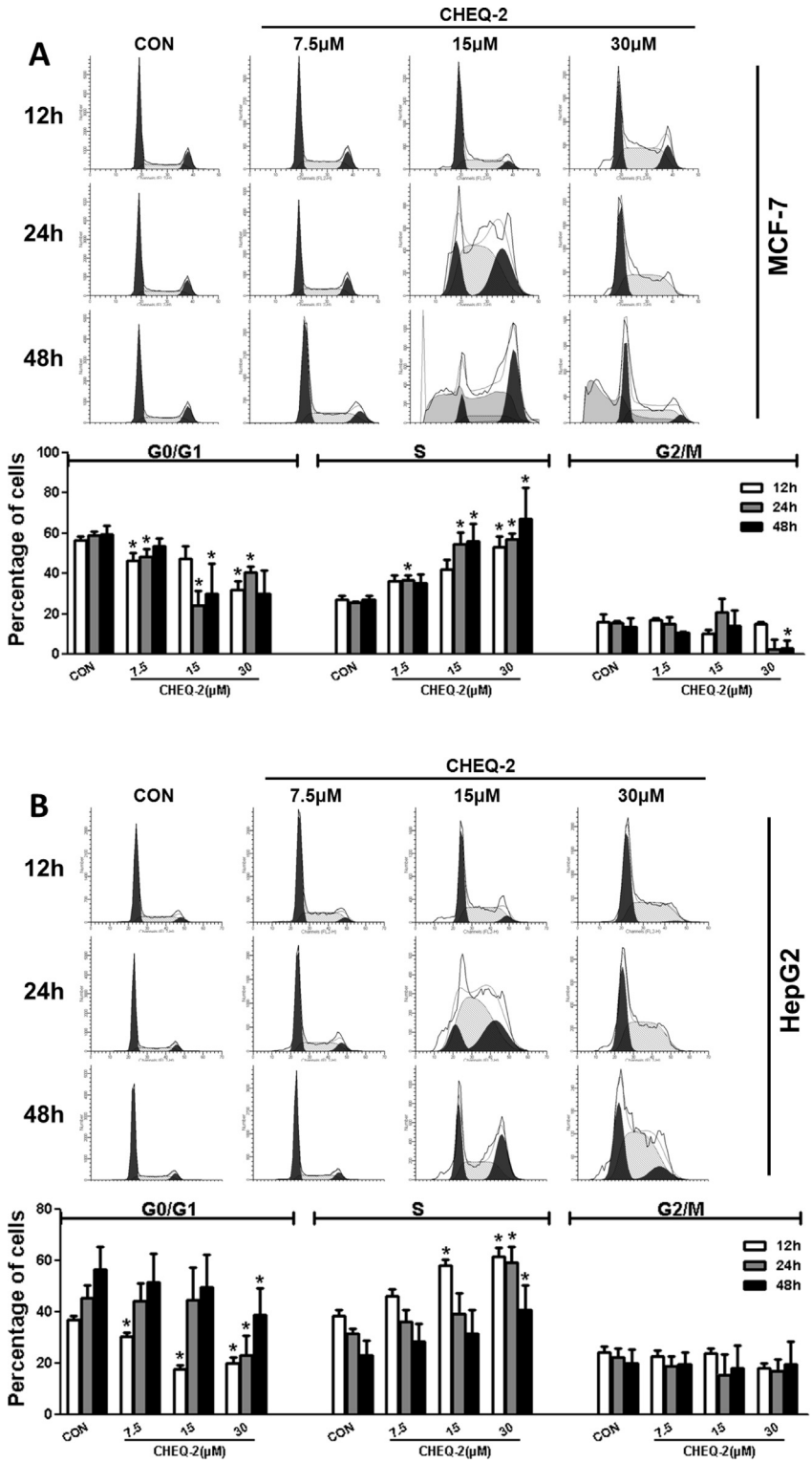

Fig. 2. CHEQ-2 induced a strong cell accumulation in S phase in MCF-7 (A), HepG2 (B) and HT-29 (C) cells. Cells were incubated with or without various concentrations of CHEQ-2 for 12 h, 24 h and 48 h. Then the cells were collected and analyzed by flow cytometry. The photographs are representatives of three independent experiments. $^{*}P < 0.05$ vs. control of the same time spot. CHEQ-2 played an important role in modulating the expression of cell cycle related proteins in MCF-7 (D), HepG2 (E) and HT-29 (F) cells. CHEQ-2 treatment caused dose-dependent downregulation of both CDC25A and CDC25B. The representative blots were shown on the left, and statistical analysis of bands intensity was shown on the right. Data were expressed as mean ± SD from three independent experiments.

However, the source of ROS formation is still remain unclear as the polyphenol structure of CHEQ-2 is most likely undergoes oxidation reaction rather than reduction action. We speculated that ROS accumulation might be a result of damaged mitochondria and disordered cell cycle, which helped to explain the reason why ROS formation in 48 h CHEQ-2 treated cells was much greater than 24 h or 12 h CHEQ-2 treated cells according to our preliminary experiment (data not shown). The generated ROS could also directly affect

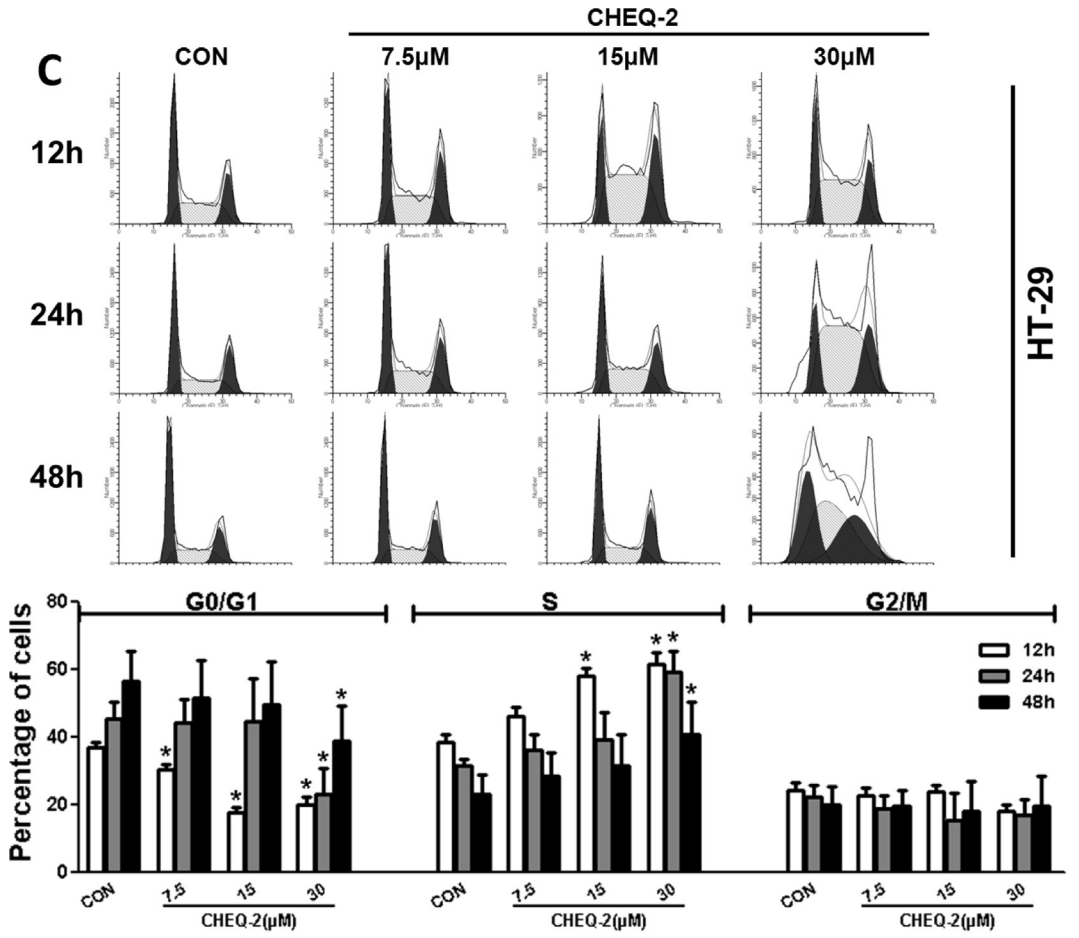

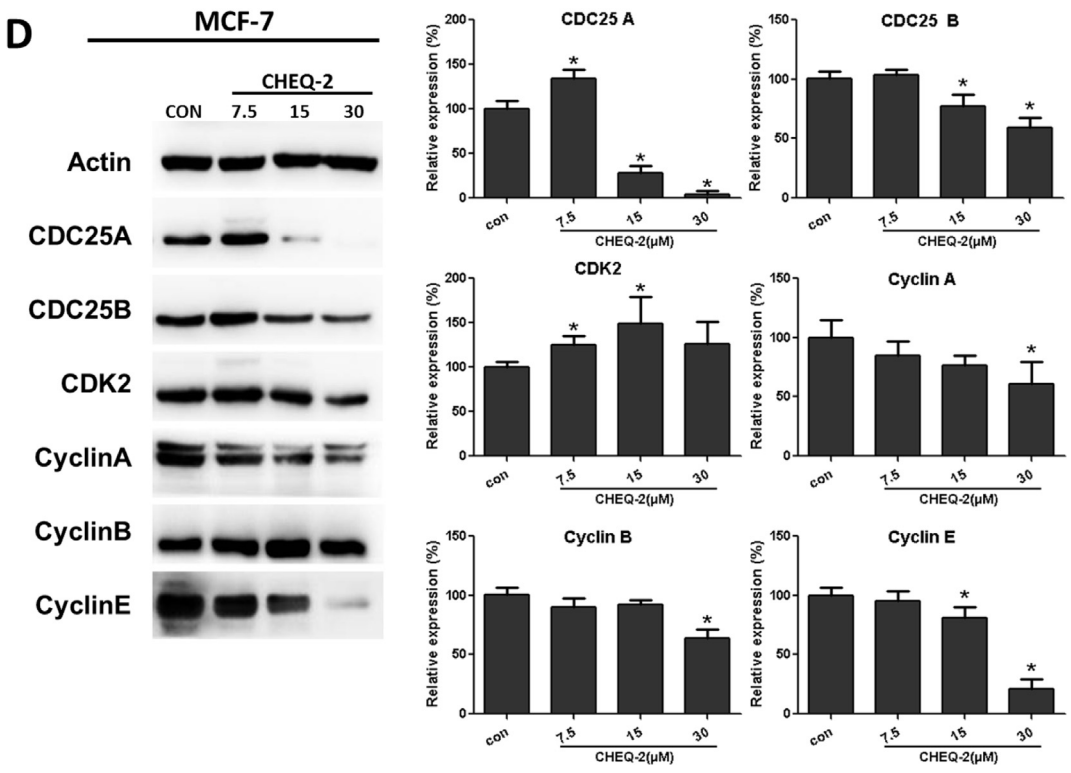

Fig. 2. (*continued*).

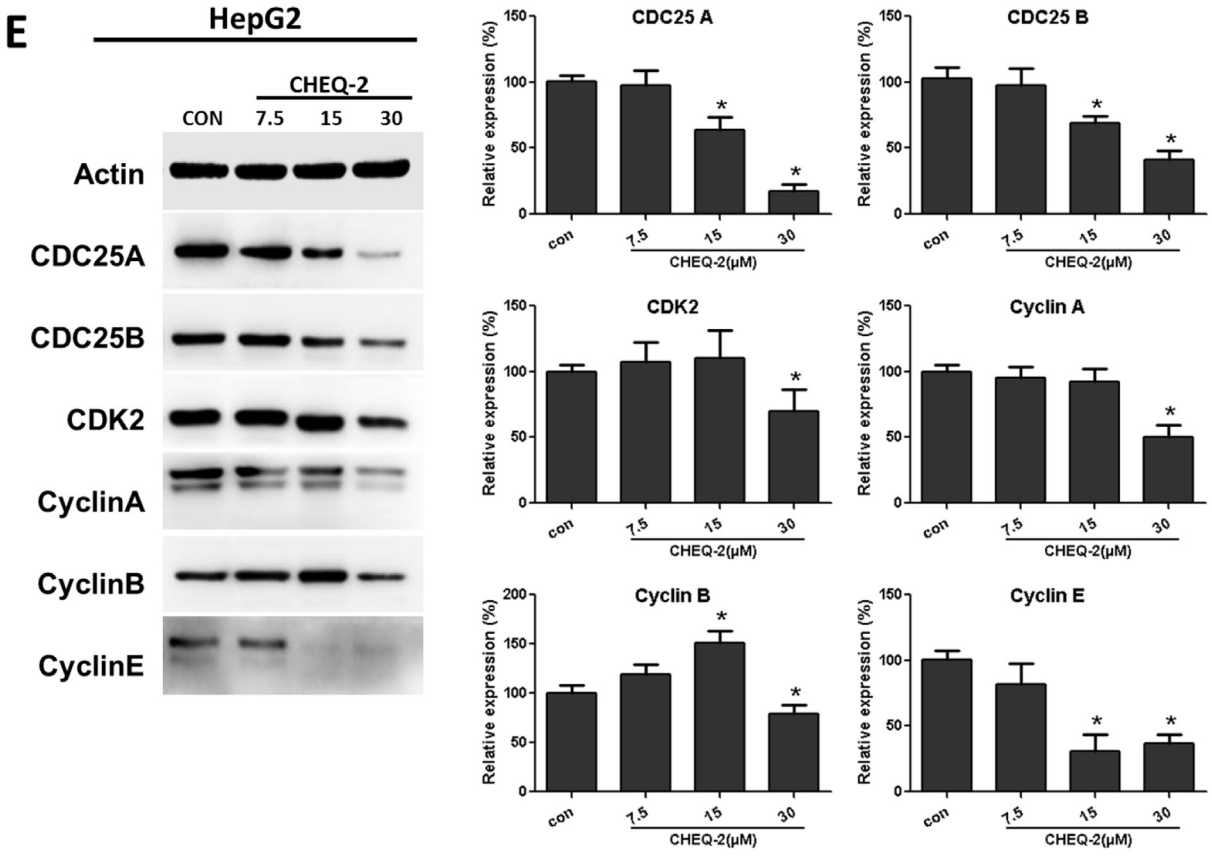

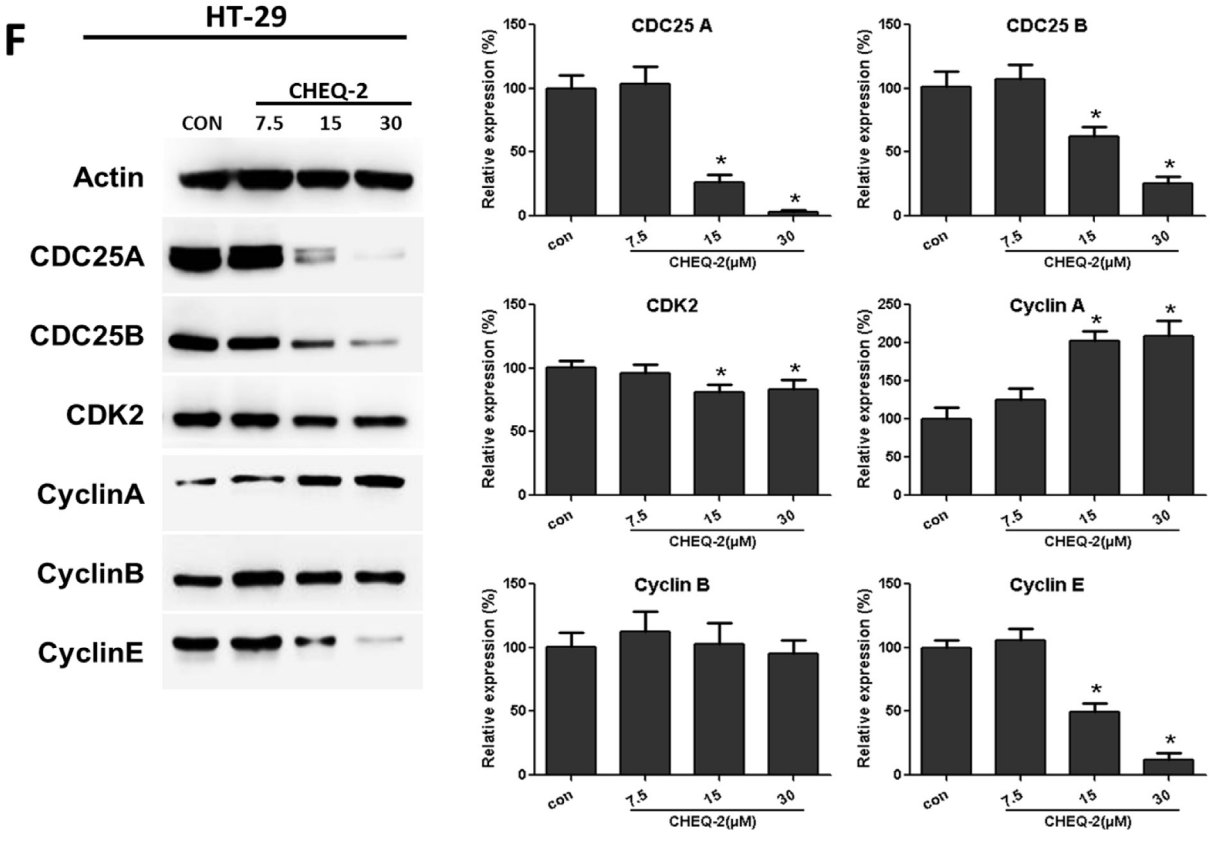

Fig. 2. (*continued*).

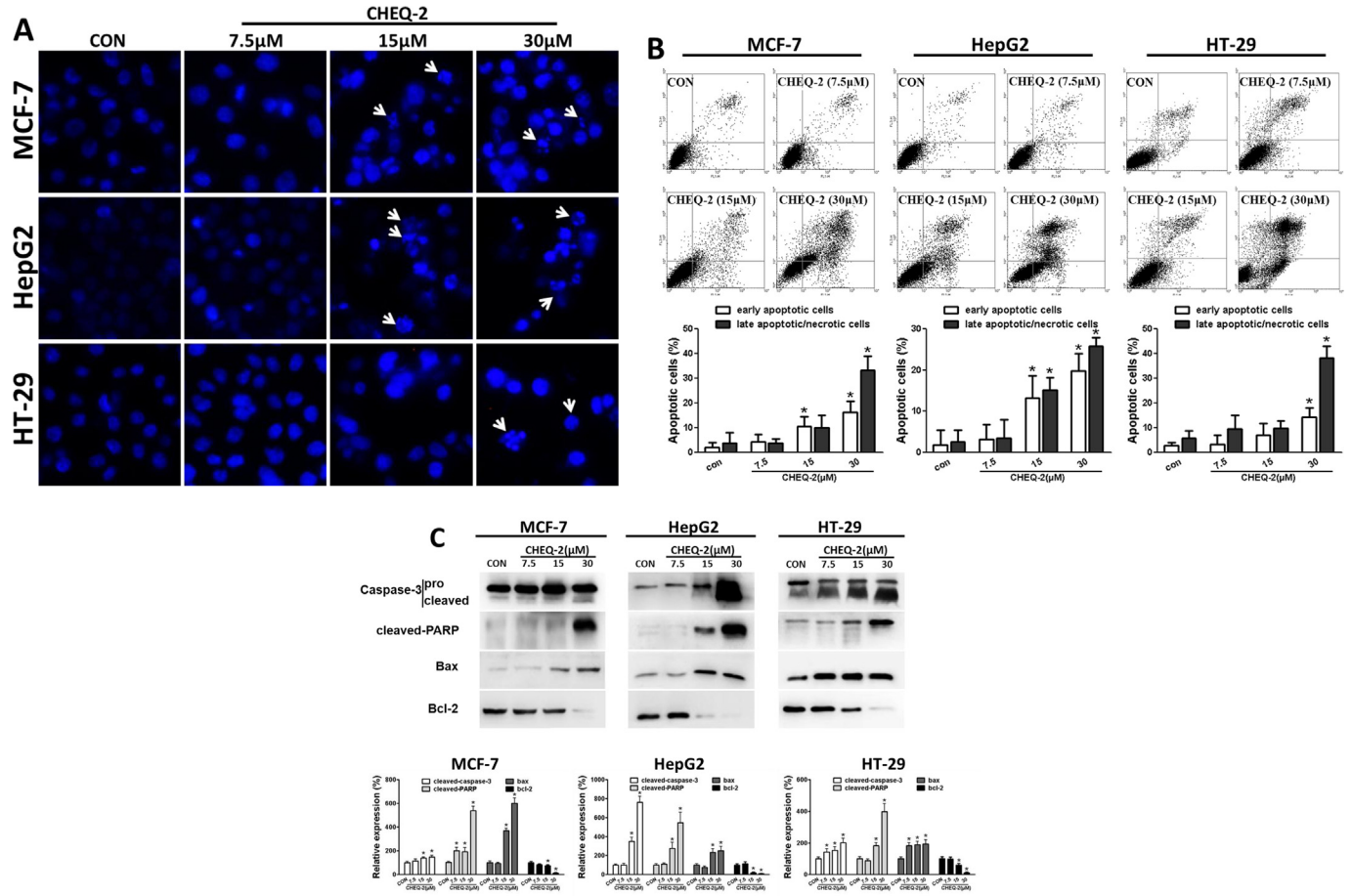

Fig. 3. CHEQ-2 induced a dramatic apoptosis in MCF-7, HepG2 and HT-29 cells. (A) Effect of CHEQ-2 on the morphology of cell nuclei. Cells were treated with or without various concentrations of CHEQ-2 for 48 h. Then the cells were collected, stained with Hoechst 33342, and the images were captured by fluorescence microscopy using identical exposure settings. Original magnification, 40×. The arrows point to the condensed and/or fragmented cell nuclei. (B) Flow cytometric analysis of the cell-surface phosphoserine. Cells were treated with or without various concentrations of CHEQ-2 for 48 h, co-stained with Annexin V–FITC and PI and analyzed by flow cytometry (FACSCalibur, BD Biosciences, USA). Early apoptotic (low right quadrant: annexin V+/PI−), late apoptotic or necrotic (upper right quadrant: annexin V+/PI+) and viable cells (low left quadrant: annexin V−/PI−) was determined and analyzed. The corresponding statistical analysis of apoptosis cells were showed at the bottom. (C) Effect of CHEQ-2 on caspase-3, cleaved PARP, bax and bcl-2 expression in MCF-7, HepG2 and HT-29 cells. All photographs are representatives of at least three independent experiments. $^{*}P < 0.05$ vs. control.

CDC25 structure, as the thiolate groups of catalytic cysteines of CDC25 phosphatases were highly reactive to oxidation [29,30]. This reaction step allowed the formation of a disulfide bond to a back-door cysteine, preventing the binding of substrate to the activesite [30,31], and therefore caused CDC25 inhibition. The duel effect of ROS highlighted the possibility of a direct link between apoptosis and cell cycle.

3.6. Acute toxicity experiment of oral administration and abdominal injection of CHEQ-2 in female BALB/c mice

There were no animal deaths in oral administration groups and only 1 death in abdominal injection CHEQ-2-treated group. Accordingly, the approximate lethal doses of CHEQ-2 in female mice are higher than 2000 mg/kg. Observed clinical signs included loss of appetite and energy in 3/4 animals after dosing for 1 or 2 days in CHEQ-2 2000 mg/kg group. The symptoms were found more serious in the abdominal injection groups, and there was also a temporary body weight drop on the second day of dosing (day 1). Other than that, normal body weight gains were observed, no significant differences were found between the vehicle control and CHEQ-2 treatment groups (Fig. 6). No abnormal gross findings were observed in any animals.

3.7. Xenografted human liver tumors in nude mice

Subcutaneous inoculation of 10^6 HepG2 cells into the left flank of nude mice resulted in the development of tumors at the site of inoculation. Daily oral administration of CHEQ-2 (10 mg/kg) was given when the tumor was well-grown. CHEQ-2-treatment resulted in apparent decrease of tumor volumes in HepG2 cells (Fig. 7A), and after a 14-day treatment with 10 mg/kg of CHEQ-2, the tumor volumes were decreased by 42.1% (Fig. 7B). As for control mice, the tumor volumes maintained steady growth momentum in the whole experiment period. The body weight of mice was consistent within 14 days of treatment with and without CHEQ-2, and no significant difference was observed (Fig. 7C). All animals showed no signs of weight loss or severe adverse action and none of the mice died during this study, suggesting that oral administration of CHEQ-2 is safe in this mouse model. The autopsy of mice did not reveal any metastatic site in both vehicle and CHEQ-2 treatment group. Compared to that of the vehicle group, the tumor weight was reduced by 43.0% in CHEQ-2-treated mice (Fig. 7D).

The expression of CDC25A, B, CDK2, and Cyclin A, B, E in the tumor tissues was further studied by western blotting. Compared with the vehicle (Fig. 7E), the CDC25A and B expression was significantly lower in the tissue from the CHEQ-2 treated mice,

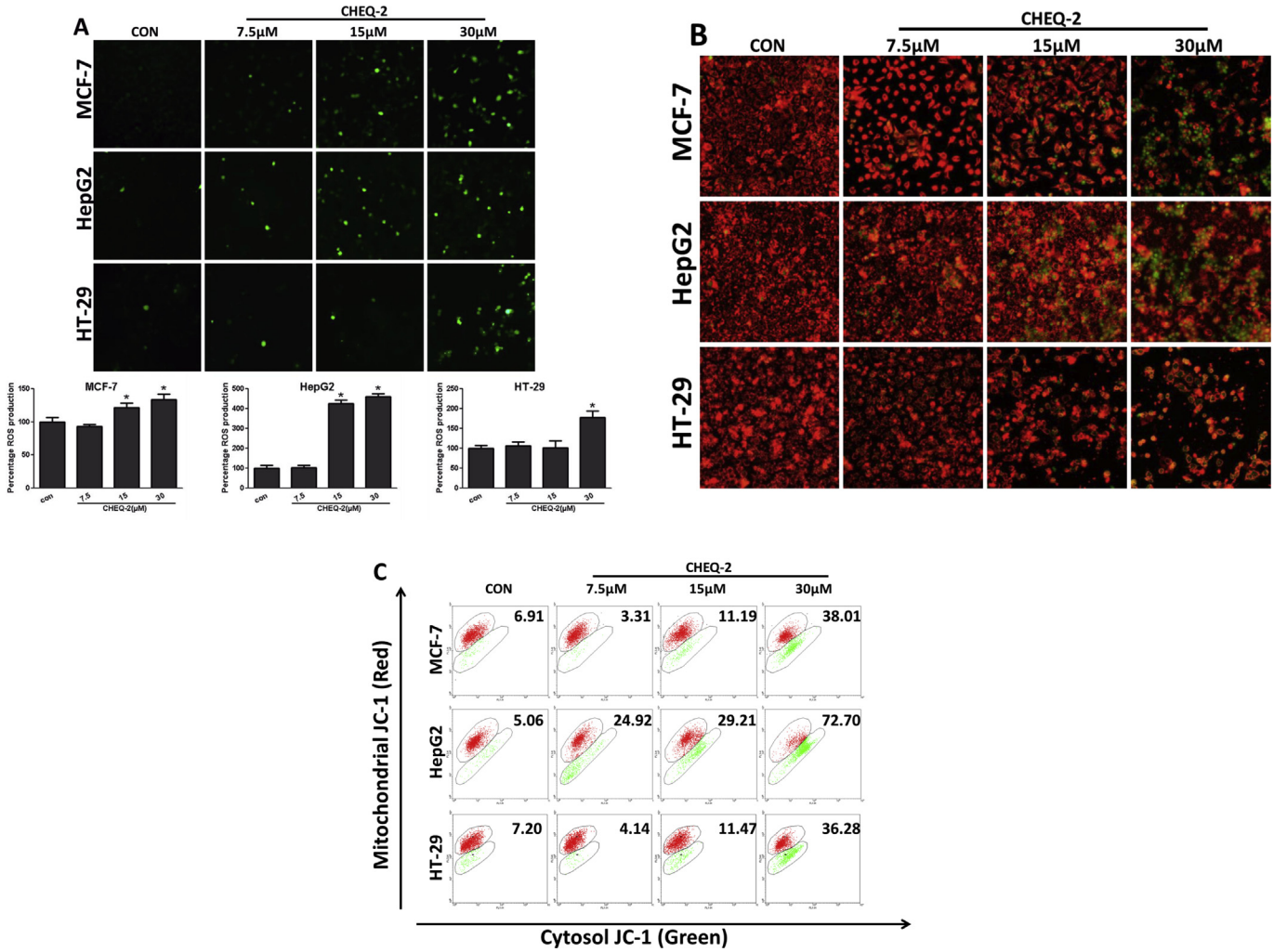

Fig. 4. CHEQ-2 increased ROS formation and triggers mitochondrial dysfunction in MCF-7, HepG2 and HT-29 cells. (A) Effect of CHEQ-2 on the formation of ROS. Cells were treated with or without various concentrations of CHEQ-2 for 48 h. The ROS levels were determined by assaying the fluorescent product 2′,7′-dichlorofluorescein (DCF) from 2′,7′-dichlorofluorescin diacetate (DCFH-DA) in viable cells. The images were captured by fluorescence microscopy using identical exposure settings. Original magnification, 20×. The statistical analysis was made on the flow cytometer. (B) Effect of CHEQ-2 on the mitochondrial membrane potential. Cells were treated with or without various concentrations of CHEQ-2 for 48 h and subsequently stained with a fluorescent dye JC-1. The cells were visualized for their green and red emission components by using optical filters designed for fluorescein and tetramethylrhodamine fluorescence microscopy (Original magnification, 20×) and statistical analysis was made by using the flow cytometer. $^{*}P < 0.05$ vs. control. (For interpretation of the references to color in this figure legend, the reader is referred to the web version of this article.)

suggesting that the CDC25 expression was also inhibited *in vivo* by CHEQ-2. Additionally, the expression of Cyclin B was also down-regulated in the tumor tissue from the mice treated with CHEQ-2. These results suggested that the inhibition of tumor growth could be indeed attributed to the suppression of CDC25A and B expression and subsequent inhibition of Cyclin B.

It was showed in this experiment that CHEQ-2 is very efficient in slowing the tumor growth. It works at a dose as low as 10 mg/kg, while LD_{50} of CHEQ-2 is over 2000 mg/kg in mice according to the acute toxicity evaluation study. It proved CHEQ-2 could be applied into use at a wide range of dosage with low toxicity. Another remarkable property of CHEQ-2-mediated tumor growth inhibition is that it remains efficient in oral dosage form, which could be enormously beneficial to its potential to be developed into a future drug. Moreover, the effect of CHEQ-2 in reducing tumor volume and weight was also observed with other doses (100 mg/kg and 1000 mg/kg). But higher doses of CHEQ-2 didn't demonstrate stronger inhibition effect on the growth of HepG2 tumor (data not shown), which may related to the drug distribution and metabolism in the animals.

4. Conclusion

In summary, the present study described the discovery and characterization of a novel CDC25A/B inhibitor, CHEQ-2, by efficient synthesis and screening of a focused compound library of the initial hit XDW-1. We provide evidence that CHEQ-2 demonstrated improved inhibitory potential compared to XDW-1 and VK3, and showed favorable inhibition on the proliferation of tumor cells. Moreover, CHEQ-2 could cause dramatic S-phase cell cycle arrest by suppressing CDC25A/B expression, eventually leads to activation of apoptosis. The CHEQ-2-treated cells also exhibited much higher ROS level and apparent decline in membrane potential, which may attribute to the cell apoptosis and could be abolished by NAC treatment. The *in vivo* approach further proved CHEQ-2 could inhibit tumor growth in nude mice with low toxicity. Over all, the data revealed that CHEQ-2 is a novel CDC25 inhibitor with remarkable tumor inhibition activities that induces cell cycle arrest, apoptosis, ROS production and mitochondrial dysfunction. With robust anticancer potencies and lower toxicity, CHEQ-2 is more effective on multiple cancer cell death than its prototype XDW-1

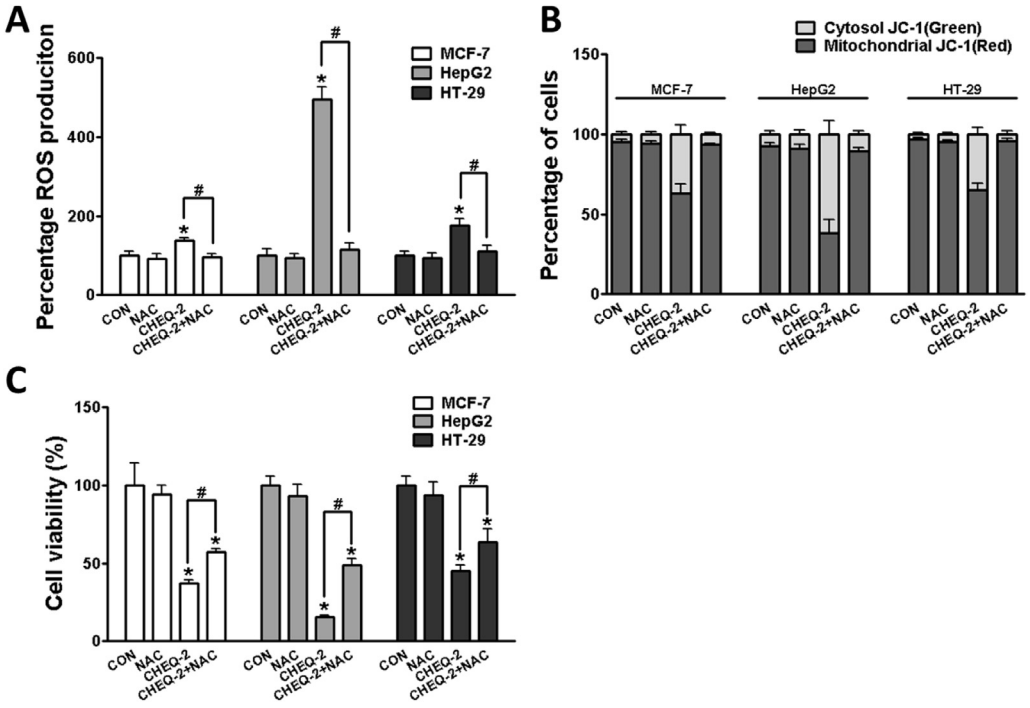

Fig. 5. ROS production, mitochondrial dysfunction and cytotoxicity effect induced by CHEQ-2 are diminished by a ROS scavenger, N-acetylcysteine (NAC). (A) NAC abrogated ROSproductioninduced by CHEQ-2 in MCF-7, HepG2 and HT-29 cells. (B) NAC abolished mitochondrial dysfunction induced by CHEQ-2 in MCF-7, HepG2 and HT-29 cells. (C) NAC could attenuate the cytotoxicity effect of CHEQ-2 in MCF-7, HepG2 and HT-29 cells. Cells were treated with or without CHEQ-2 (30 μM) at the presence or absence of NAC (5 mM) for 48 h. Data were expressed as mean ± SD from at least three independent experiments. $^{*}P < 0.05$ vs. control. #$P < 0.05$ vs. CHEQ-2 alone.

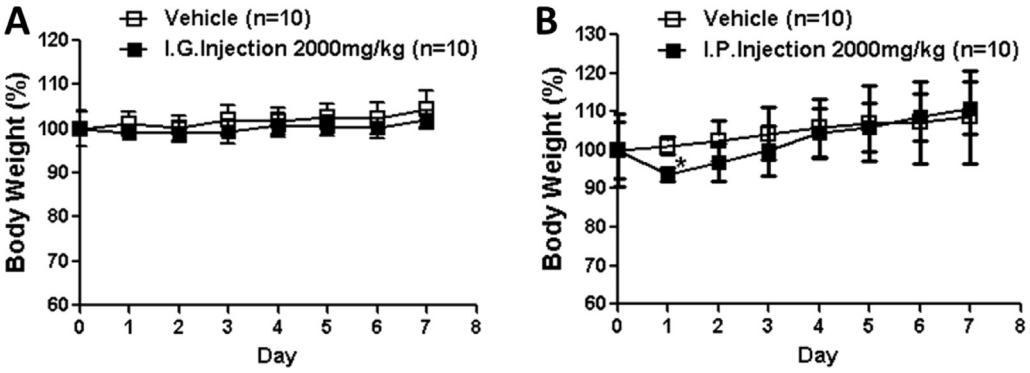

Fig. 6. CHEQ-2 showed extremely low acute toxicity in BALB/c mice (female). (A) Changes of body weights in the tested animals after one time I.G. injection of CHEQ-2 (2000 mg/kg). (B) Changes of body weights in the tested animals after one time I.P. injection of CHEQ-2 (2000 mg/kg). $^{*}P < 0.05$ vs. control.

and positive compound VK3. Therefore, this compound deserves further investigation in the hope of providing new alternatives to treat cancer patients.

5. Experimental section

5.1. Synthesis procedure

All melting points were determined on a micromelting point apparatus and are uncorrected. ^{1}H NMR and ^{13}C NMR spectra were obtained on a Bruker Avance-400NMR-spectrometer in the indicated solvents. Chemical shifts are expressed in δ units and TMS as internal reference. Mass spectra were taken on a LC Autosampler Device: Standard G1313A instrument. TLC was performed on Silica Gel GF254 for TLC and spots were visualized by iodine vapors or by irradiation with UV light (λ = 254 nm). Flash column chromatography was performed on column packed with Silica Gel60 (230–400 mesh). Solvents were reagent grade, when necessary, were purified and dried by standard methods. Concentration of the reaction solutions involved the use of rotary evaporator at reduced pressure.

5.1.1. Preparation of 2-(4-(4-chlorophenyl)-5-p-tolyl-4H-1,2,4-triazol-3-ylthio)-1-(3,4-dihydroxyphenyl)ethanone (4, XDW-1)

To a cooled solution of 1,2-dichloroethane (20 mL) at about 5–10 °C, aluminum chloride (6.0 g, 45 mmol) was added, then the mixture solution was stirred at 5–10 °C for about 30 min. Then catechol (**1**) (2.0 g, 18.1 mmol) was added portion wise to the stirred reaction mixture within about 10 min and the reaction mixture was further stirred for 20 min. To the above solution, chloroacetyl chloride (2.2 g, 19.3 mmol) was added at 5–10 °C. Then the temperature was raised to room temperature and with further stirring

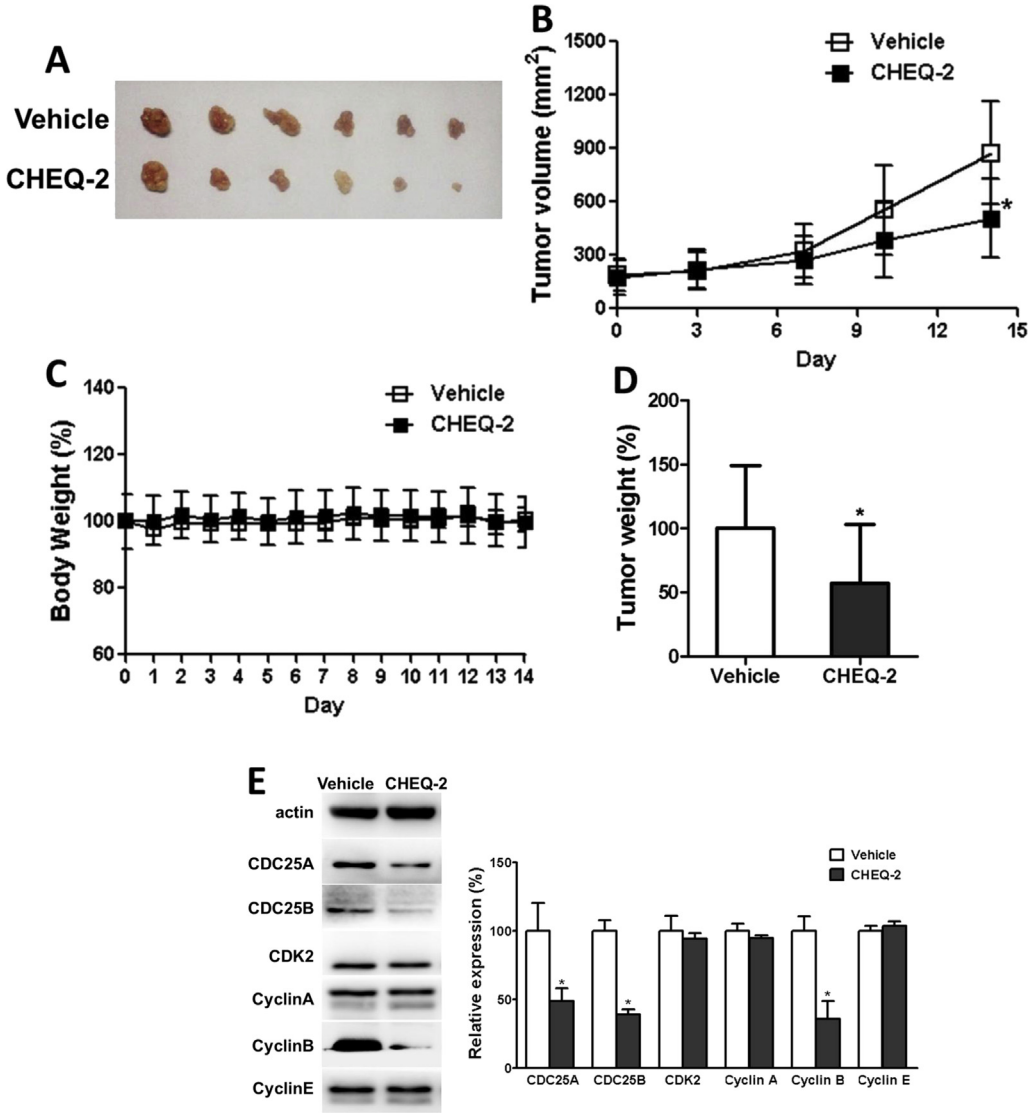

Fig. 7. CHEQ-2 inhibited tumor growth from hepatocellular carcinoma cells HepG2 in nude mice. (A) Photographs of tumor removed from nude mice after 14 days of vehicle or CHEQ-2 treatment. 1×10^7 HepG2 cells were injected s.c. into the left flanks of 6-week-old female nude mice ($n = 6$). Vehicle or CHEQ-2 (10 mg/kg) were given orally once a day for 2 weeks when the tumor were grown (length × width > 100 mm^2). Tumor volume (B) was measured on day 0, 3, 7, 10, 14 and body weight (C) was measured every single day. (D) The tumors were weighed after sacrifice and the inhibitory effect was defined as a percentage of vehicle control tumor weight. All the data were obtained from 6 Balb/c nude mice. $^*P < 0.05$ vs. vehicle control. (E) CHEQ-2 treatment induced downregulation of CDC25A, CDC25B and Cyclin B in xenograft tumors. A small piece (approximately 0.05 g) was taken from each collected tumor and homegenated to form a mixture. Then the protein was extracted and assayed by western blotting. Data were expressed as mean ± SD. $^*P < 0.05$ vs. control.

for about 20 h. After completion of the reaction, the reaction was quenched with dilute hydrochloric acid solution (40 mL) at 5–10 °C and stirred for 2–3 h at room temperature. The obtained solid was filtered and washed with water. The wet solid was suspended in dilute acetic acid and heated to get a clear solution. To this clear solution, carbon (0.1 g) was added and stirred for 30 min. The reaction mixture was filtered in hot. The filtrate was cooled and the formed solid was filtered and washed with water. It was dried to obtain the product 2-chloro-1-(3,4-dihydroxyphenyl)ethanone (**2**). Yield: 2.5 g, 74%; M.P. 175–177 °C.

To a solution of the 4-(4-chlorophenyl)-5-p-tolyl-4H-1,2,4-triazole-3-thiol (**3**) (CAS No. 451501-95-4) (0.6 g, 1.99 mmol) in acetone (30 mL) was added K_2CO_3 (0.3 g, 2.17 mmol) followed by 2-chloro-1-(3,4-dihydroxyphenyl)ethanone (**2**) (0.35 g, 1.88 mmol). The resulting solution was stirred at room temperature for 14 h, diluted with water and extracted with EtOAc. The organic layer was washed with water, dried on anhydrous Na_2SO_4, then filtered and evaporated under reduced pressure to afford white solid as crude product. Then recrystallization of the crude product in ethanol/petroleum(60–90) gave the purified product 2-(4-(4-chlorophenyl)-5-p-tolyl-4H-1,2,4-triazol-3-ylthio)-1-(3,4-dihydroxyphenyl)ethanone (**XDW-1, 4**) as white solid. Yield: 0.20 g, 23.5%; $R_f = 0.50$ (petroleum 60–90/EtOAc, 1:1). ^{1}H NMR (400 MHz, DMSO-d6, ppm) δ: 9.71 (2H, brs, 2 × OH), 7.62 (2H, d, $J = 8.6$ Hz), 7.46 (2H, d, $J = 8.7$ Hz), 7.44 (1H, dd, $J = 8.7$, 2.4 Hz), 7.36 (1H, d, $J = 2.4$ Hz), 7.23 (2H, d, $J = 8.2$ Hz), 7.17 (2H, d, $J = 8.2$ Hz), 6.84 (1H, d, $J = 8.2$ Hz), 4.80 (2H, s, S–CH_2), 2.28 (3H, s, Me). ESI-MS: m/z 452.3 (M+1), 454.4 (M+3). $C_{23}H_{18}ClN_3O_3S$ (451.076).

5.1.2. Preparation of 1-(3,4-dihydroxyphenyl)-2-((1-mesityl-1H-imidazo[4,5-c] pyridin-2-yl)thio)ethanone (CHEQ-2, 9a)

Compound 4-chloro-3-nitropyridine (**5a**) (1.58 g, 10 mmol), $NaHCO_3$ (2.52 g, 30 mmol) and 2,4,6-trimethylbenzenamine (1.50 g, 11 mmol), were dissolved in alcohol (25 mL). The reaction

mixture was heated to reflux temperature with stirring and kept for 10 h and then continued the reaction at room temperature for another 12 h (monitored by TLC). The reaction liquid was evaporated under reduced pressure. Then, the residue was dissolved with a small amount DCM (CH_2Cl_2) and chromatographed on silica gel using ethyl acetate–petroleum ether system. Pure fractions were collected and concentrated to give **6a** as a yellow solid, yield: 59.2%, mp: 133–139 °C. MS (ESI): *m/z* 258.12 (M+1). $C_{14}H_{15}N_3O_2$ (257.12).

The reaction intermediate **6a** (3 g, 12 mmol), Pd/C (0.1 g) and 25 mL alcohol was vacuumed and filled with excess hydrogen gas. The reaction mixture was kept for 15 h and then filtered and evaporated under reduced pressure. The obtained crude product was washed with petroleum ether and evaporated under reduced pressure again to give the purified compound **7a**. Brown powder, yield: 81%. mp: 187–192 °C. MS (ESI): *m/z* 228.6. $C_{14}H_{17}N_3$ (227.14).

Intermediate **7a** (0.6 g, 2.6 mmol), $EtOCS_2K$ (0.5 g, 3.1 mmol) and $NaHCO_3$ (0.05 g, 0.6 mmol) were dissolved in alcohol (10 mL) and water (3 mL), then the solution was refluxed for 5 h. The reaction liquid was cooled to room temperature and then 20 mL water and 8 mL NaOH solution (2 M) was added. The formed precipitate was removed by suction filtration and the filtrate was modulated to PH 7 by adding acetic acid. 1-Mesityl-1H-imidazo[4,5-c]pyridine-2-thiol (**8a**) was precipitated, filtered by suction filtration and air-dried to yield a yellowish-white powder. Yield: 83.2%. mp: 247–250 °C. MS (ESI): *m/z* 270.7. $C_{15}H_{15}N_3S$ (269.1).

Compound **8a** (0.269 g, 1.0 mmol), K_2CO_3 (0.138 g, 1.0 mmol), with 2-chloro-1-(3,4-dihydroxyphenyl)ethanone (**2**) (0.186 g, 1.0 mmol) were dissolved in acetone (10 mL). The reaction mixture was stirred at room temperature for 7 h and then evaporated under reduced pressure. Then the residue was poured into water (30 mL) at room temperature and a large amount of gray precipitation was obtained. Filtration and recrystallization the precipitation in ethanol yielded the purified product1-(3,4-dihydroxyphenyl)-2-((1-mesityl-1H-imidazo[4,5-c]pyridin-2-yl)thio)ethanone (**CHEQ-2**, **9a**) as gray power. Yield: 0.283 g, 67%; mp: 256–258 °C. ^{1}H NMR (400 MHz, DMSO-d6, ppm) δ: 9.78 (2H, brs), 8.88 (1H, s, C_4-imidazo [4,5-c]pyridine-H), 8.26 (1H, d, J = 4.8 Hz, C_6-imidazo[4,5-c]pyridine-H), 7.49 (1H, dd, J = 1.5, 8.2 Hz, C_6-Ph′-H), 7.41 (1H, s, C_2-Ph′-H), 7.19 (2H, s, $C_{3,5}$-Ph-H), 6.97 (1H, d, J = 4.8 Hz, C_7-imidazo[4,5-c] pyridine-H), 6.86 (1H, d, J = 8.2 Hz, C_5-Ph′-H), 5.03 (2H, s, S–CH_2), 2.38 (3H, s, Me), 1.88 (6H, s, 2 × Me). ^{13}C NMR (100 MHz, DMSO-d6, ppm) δ: 190.1, 155.1, 152.2, 146.0, 142.5, 141.2, 140.8, 140.5, 140.1, 136.7 (2 × C), 130.1 (2 × C), 129.0, 127.4, 122.4, 115.7, 115.5, 105.0, 21.2, 17.4 (2 × C). MS (ESI): *m/z* 420.3 (M+1). $C_{23}H_{21}N_3O_3S$ (419.13).

5.1.3. Preparation of 1-(3,4-dihydroxyphenyl)-2-(3-mesityl-3H-imidazo[4,5-b] pyridin-2-ylthio)ethanone (CHEQ-1, 9b)

The reaction mixture of 2-chloro-3-nitropyridine (**5b**) (0.79 g, 5 mmol), 2,4,6-trimethylben-zenamine (2.7 g, 20 mmol), and KF (0.47 g, 8 mmol) was slowly heated to reflux temperature with stirring and continued for another 12 h (monitored by TLC). The suspension was cooled to room temperature and then poured into 80 mL water and 10 mL ammonia. The mixture was then extracted with CH_2Cl_2 (15 mL), washed successively with water (3 × 10 mL). The organic layer was dried over anhydrous Na_2SO_4, filtered and concentrated under reduced pressure to afford crude product **6b** as brown oil. And then the crude product was purified by recrystallization from alcohol–petroleum ether to give **6b** as yellow needle crystals, yield: 67%, MS (ESI): *m/z* 258.12 (M+1). $C_{14}H_{15}N_3O_2$ (257.12). Then, compound N^2-mesitylpyridine-2,3-diamine (**7b**) was prepared from **6b** using a similar procedure described for the preparation of **7a.** Gray powder, yield: 69%. mp: 181–184 °C. MS (ESI): *m/z* 228.6. $C_{14}H_{17}N_3$ (227.14). Compound 3-mesityl-3H-imidazo[4,5-b] pyridine-2-thiol (**8b**) was prepared using a similar procedure described for the preparation of **8a**. Gray powder, yield: 63%. mp: 247–253 °C. MS(ESI): *m/z* 270.7. $C_{15}H_{15}N_3S$ (269.1).

To a solution of compound **8b** (0.27 g, 1.0 mmol) in acetone (20 mL) was added K_2CO_3 (0.14 g, 1.0 mmol) followed by 2-chloro-1-(3,4-dihydroxyphenyl)ethanone (**2**) (0.18 g, 0.96 mmol). The resulting solution was stirred at room temperature for 10.5 h, diluted with water and extracted with EtOAc. The organic layer was washed with water, dried on anhydrous Na_2SO_4, then filtered and evaporated under reduced pressure to afford the crude product as white solid. Then recrystallization of the crude product in ethanol gave the purified product1-(3,4-dihydroxyphenyl)-2-(3-mesityl-3H-imidazo[4,5-b]pyridin-2-ylthio)ethanone (**CHEQ-1, 9b**) as white solid. Yield: 0.27 g, 67.0%; R_f = 0.6 (petroleum 60–90/EtOAc, 1:1). ^{1}H NMR (400 MHz, DMSO-d6, ppm) δ: 10.00 (1H, s, OH), 9.44 (1H, s, OH), 8.13 (1H, dd, J = 4.1 Hz, C_7-imidazo[4,5-b]pyridine-H), 7.96 (1H, dd, J = 7.76 Hz, C_5-imidazo[4,5-b]pyridine-H), 7.49 (1H, d, J = 7.88 Hz, C_6-Ph′-H), 7.42 (1H, s, C_2-Ph′-H), 7.24 (1H, dd, J = 2.4, 7.3 Hz, C_6-imidazo[4,5-b]pyridine-H), 7.14 (2H, s, $C_{3,5}$-Ph-H), 6.86 (1H, d, J = 7.0 Hz, C_5-Ph′-H), 4.99 (2H, s, S–CH_2), 2.37 (3H, s, Me), 1.87 (6H, s, 2 × Me). MS (ESI): *m/z* 420.3 (M+1). $C_{23}H_{21}N_3O_3S$ (419.13).

5.1.4. Preparation of N-(2-aminophenyl)-2-((1-mesityl-1H-imidazo [4,5-c]pyridin-2-yl) thio)acetamide (CHEQ-3, 13a) (Scheme 3)

The starting material 2-nitroaniline **(10)** (2.0 g, 14.5 mmol) was dissolved in DCM (15 mL), then Et_3N (2.5 mL, 17.4 mmol) was added and stirred for 10 min. Then the mixed solution of 2-chloroacetyl chloride (1.38 mL, 17.4 mmol) in DCM (10 mL) was slowly added to the above solution within 40 min. The reaction mixture was stirred for 3 h. Ice water (40 mL) was added to the reaction solution, then the solution was extracted with DCM (3 × 15 mL). Combined organic phase was dried over anhydrous Na_2SO_4, filtered and concentrated under reduced pressure to give the product 2-chloro-N-(2-nitrophenyl) acetamide **(11)** as a yellow crystal with a yield of 83.6%. Then Fe (0.56 g, 10 mmol), NH_4Cl (0.06 g, 1 mmol), HOAc (0.12 mL, 2 mmol) were added into 5 mL H_2O and stirred at 50 °C for 15 min. A solution of 2-chloro-N-(2-nitrophenyl)acetamide (0.21 g, 1 mmol) in DMF (5 mL) was added into the above solution quickly, and stirring was continued at 50 °C for 15 min. Then the reaction solution was alkalized to pH = 9 with aqueous sodium carbonate solution. The reaction mixture was filtered, the formed solid was washed with water and ethyl acetate. The combined filtrate was extracted with ethyl acetate. Then the combined organic layers were washed with brine, dried over anhydrous Na_2SO_4, filtered, concentrated under reduced pressure. Purification of the crude product by flash chromatography on silica gel (petroleum ether/ethyl acetate, 1/1) to give the N-(2-aminophenyl)-2-chloroacetamide (**12**) as a gray solid. Yield: 72.5%.

Compound **8a** (0.15 g, 0.5 mmol), K_2CO_3 (0.14 g, 1.0 mmol), and the intermediate **12** (0.12 g, 0.6 mmol) were dissolved in DMF (10 mL). The reaction mixture was stirred at room temperature for 5 h and then evaporated under reduced pressure. The residue was washed by water, then extracted with ethyl acetate (3 × 50 mL). Combined organic phase was dried over anhydrous Na_2SO_4, filtered and chromatographed on silica gel using ethyl acetate–petroleum ether system. Pure fractions were collected and concentrated and recrystallized from EtOAc/petroleum 60–90 to give the desired compound N-(2-aminophenyl)-2-((1-mesityl-1H-imidazo[4,5-c] pyridin-2-yl)thio) acetamide (**CHEQ-3, 13a**) as white crystal. Yield 65.5%, mp: 154–158 °C. ^{1}H NMR (400 MHz, DMSO-d6, ppm)δ: 9.60 (1H, s, NH), 8.92 (1H, s, C_4-imidazo[4,5-c]pyridine-H), 8.28 (1H, d, J = 5.4 Hz, C_6-imidazo[4,5-c]pyridine-H), 7.18 (2H, s, $C_{3,5}$-Ph-H),7.09 (1H, dd, J = 7.72, 0.92 Hz, C_6-Ph′-H), 6.97 (1H, d, J = 5.44 Hz, C_7-imidazo[4,5-c]pyridine-H), 6.92 (1H, td, J = 7.92, 1.2 Hz, C_4-Ph′-H), 6.71 (1H, dd, J = 7.92, 0.8 Hz, C_3-Ph′-H), 6.52 (1H, td, J = 7.68,

0.92 Hz, C_5-Ph′-H), 5.08 (2H, s, NH_2), 4.33 (2H, s, S–CH_2), 2.36 (3H, s, Me), 1.85 (6H, s, 2 × Me). ^{13}C NMR (100 MHz, DMSO-d6, ppm) δ: 166.1, 155.2, 143.4, 142.6, 141.1, 140.7, 140.6, 140.0, 136.7 (2 × C), 130.1 (2 × C), 128.9, 127.0, 126.6, 122.9, 116.3, 115.8, 105.1, 36.1, 21.2, 17.4 (2 × C). ESI-MS: *m*/*z* 418.5 (M+1), 420.3 (M+3), 440.5 (M+Na). $C_{23}H_{23}N_5OS$ (417.53).

5.1.5. Preparation of N-(2-aminophenyl)-2-((3-mesityl-3H-imidazo [4,5-b]pyridin- 2-yl)thio)acetamide (CHEQ-4, 13b)

Compound **CHEQ-4** (**13b**) was synthesized from *N*-(2-aminophenyl)-2-chloroacetamide (**12**) and compound **8b** according to the procedure of **CHEQ-3** (**13a**). White crystal, yield 71.3%, mp: 165–167 °C. ^{1}H NMR (400 MHz, DMSO-d6, ppm) δ: 9.57 (1H, s, NH), 8.16 (1H, dd, *J* = 4.63, 0.8 Hz, C_7-imidazo[4,5-b]pyridine-H), 8.01 (1H, dd, *J* = 7.92, 0.92 Hz, C_5-imidazo[4,5-b]pyridine-H), 7.29 (1H, dd, *J* = 7.96, 6.05 Hz, C_6-Ph′-H), 7.13 (2H, s, $C_{3,5}$-Ph-H), 7.09(1H, d, *J* = 7.72, 0.92 Hz, C_6-imidazo[4,5-b]pyridine-H), 6.92 (1H, td, *J* = 8.04, 1.04 Hz, C_4-Ph′-H), 6.70 (1H, d, *J* = 7.24 Hz, C_3-Ph′-H), 6.52 (1H, td, *J* = 7.68, 0.52 Hz, C_5-Ph′-H), 5.04 (2H, s, NH_2), 4.33 (2H, s, S–CH_2), 2.36 (3H, s, Me), 1.85 (6H, s, 2 × Me). ^{13}C NMR (100 MHz, DMSO-d6, ppm) δ: 166.2, 154.7, 149.3, 143.3, 143.2, 140.1, 136.9 (2C), 135.5, 129.7 (2C), 129.4, 126.9, 126.4, 125.4, 123.1, 118.8, 116.4, 115.9, 35.6, 21.2, 17.6 (2C). ESI-MS: *m*/*z* 418.5 (M+1), 420.3 (M+3), 440.5 (M+Na). $C_{23}H_{23}N_5OS$ (417.53).

5.1.6. Preparation of N-(2-hydroxyphenyl)-2-((1-mesityl-1H-imidazo[4,5-c] pyridin- 2-yl)thio)acetamide (CHEQ-5, 16a)

The starting material 2-aminophenol **(14)** (1.0 g, 9.16 mmol) was dissolved in 1,2-dichloroethane (8 mL). Then the mixed solution of 2-chloroacetyl chloride (1.53 mL, 19.2 mmol) and chloroacetic acid (0.06 mL, 0.96 mmol), 1,2-dichloroethane (5 mL) was slowly added to the above solution in 50 min. Then the mixture was refluxed for 3 h, and then cooled to room temperature. A large amount of precipitation of crystallization was formed, filtered and recrystallized from 1,2-dichloroethane to give the N-(2-hydroxyphenyl)-2-chloroacetamide (**15**) as brown crystal. Yield: 90.3%.

Compound **8a** (0.15 g, 0.5 mmol), K_2CO_3 (0.14 g, 1.0 mmol), and compound **15** (0.12 g, 0.6 mmol), was dissolved in DMF (10 mL). The reaction mixture was stirred at room temperature for 5 h and then evaporated under reduced pressure. The residue was washed by water, then extracted with ethyl acetate (3 × 50 mL). Combined organic phase was dried over anhydrous Na_2SO_4, filtered and chromatographed on silica gel using ethyl acetate–petroleum ether system. Pure fractions were collected, concentrated, and recrystallized from EtOAc/petroleum 60–90 to give N-(2-hydroxyphenyl)-2-((1-mesityl-1H-imidazo[4,5-c]pyridin-2-yl) thio)acetamide **(CHEQ-5, 16a)** as white crystal. Yield 68.9%, mp: 231–233 °C. ^{1}H NMR (400 MHz, DMSO-d6, ppm) δ: 9.96 (1H, s, NH), 9.84(1H, s, OH), 8.96 (1H, s, C_4-imidazo[4,5-c]pyridine-H), 8.28 (1H, d, *J* = 5.44 Hz, C_6-imidazo[4,5-c]pyridine-H), 7.93(1H, dd, *J* = 8.0, 1.12 Hz, C_6-Ph′-H), 7.18 (2H, s, $C_{3,5}$-Ph-H), 6.98 (1H, d, *J* = 5.44 Hz, C_7-imidazo[4,5-c]pyridine-H), 6.92 (1H, td, *J* = 8.12, 1.36 Hz, C_4-Ph′-H), 6.85 (1H, dd, *J* = 7.92, 1.24 Hz, C_3-Ph′-H), 6.74 (1H, td, *J* = 7.12, 1.28 Hz, C_5-Ph′-H), 4.35 (2H, s, S–CH_2), 2.36 (3H, s, Me), 1.85 (6H, s, 2 × Me). ^{13}C NMR (100 MHz, DMSO-d6, ppm) δ: 166.2, 155.0, 147.8, 142.7, 141.3, 140.6, 140.5, 140.3, 136.6 (2 × C), 130.1 (2 × C), 128.8, 126.7, 124.8, 121.4, 119.3, 115.5, 105.1, 36.1, 21.2, 17.4 (2 × C). ESI-MS: *m*/*z* 419.4 (M+1), 422.6 (M+3), 441.4 (M+Na). $C_{23}H_{22}N_4O_2S$ (418.51).

5.1.7. Preparation of N-(2-hydroxyphenyl)-2-((3-mesityl-3H-imidazo[4,5-b] pyridine-2-yl)thio)acetamide (CHEQ-6, 16b)

Compound **CHEQ-6** (**16b**) was synthesized from *N*-(2-hydroxyphenyl)-2-chloroacetamide (**15**) and compound **8b** according to the procedure of **CHEQ-5** (**16a**). White crystal, yield 69.7%, mp: 181–184 °C. ^{1}H NMR (400 MHz, DMSO-d6, ppm) δ: 9.92 (1H, s, NH), 9.82 (1H, s, OH), 8.16 (1H, dd, *J* = 4.80, 1.28 Hz, C7-imidazo[4,5-b]pyridine-H), 8.05 (1H, dd, *J* = 7.96, 1.28 Hz, C5-imidazo[4,5-b] pyridine-H), 7.93 (1H, dd, *J* = 8.04, 1.24 Hz, C6-Ph′-H), 7.31 (1H, dd, *J* = 7.96, 4.84 Hz, C6-imidazo[4,5-b]pyridine-H), 7.93 (2H, s, C3,5-Ph-H), 6.92 (1H, td, *J* = 8.20, 1.40 Hz, C4-Ph′-H), 6.85 (1H, dd, *J* = 7.88, 1.20 Hz, C3-Ph′-H), 6.75 (1H, td, *J* = 8.12, 1.28 Hz, C3-Ph′-H), 4.34 (2H, s, S–CH_2), 2.36(3H, s, Me), 1.85 (6H, s, 2 × Me). ^{13}C NMR (100 MHz, DMSO-d6, ppm) δ: 166.3, 154.4, 149.4, 147.7, 143.4, 140.1, 136.9 (2 × C), 135.4, 129.7 (2 × C), 129.3, 126.7, 125.7, 124.8, 121.5, 119.4, 118.9, 115.5, 35.4, 21.2, 17.6 (2 × C). ESI-MS: *m*/*z* 419.4 (M+1), 422.6 (M+3), 441.4 (M+Na). $C_{23}H_{22}N_4O_2S$ (418.51).

5.2. Biological evaluations

5.2.1. Drugs and biochemicals

VK3 was purchased from Sigma Chemical Company (Sigma, USA). Stock solutions (5 mM) of VK3, XDW-1 and CHEQ-1~CHEQ-6 were prepared in DMSO and stored at −20 °C for less than 2 weeks. All chemicals were of the purest reagent grade commercially available. All cell culture reagents were from Gibco BRL (Gibco, USA). Monoclonal anti-CDC25A, anti-Cyclin E, anti-caspase-3, anti-Bax and anti-Bcl-2 antibodies were purchased from Cell Signaling Technology Inc. (CST, USA) and anti-CDC25B, anti-CDK2 anti-Cyclins (A and B) and anti-cleaved-PARP antibodies were purchased from Abcam (Abcam, USA). Protein concentrations were determined using a bicinchoninic acid (BCA) protein determination kit from Thermo Scientific Pierce (Thermo, USA).

5.2.2. Cell lines and cell culture

Human colon cancer HT-29 cells, breast cancer MCF-7 cells and hepatocellular carcinoma HepG2 cells and all the other cells used in the experiment were purchased from the Type Culture Collection of the Chinese Academy of Sciences, Shanghai, China. HT-29 cells were cultured in McCOY's 5A medium, while MCF-7 and HepG2 cells were cultured in MEM medium. The other cell lines were maintained in the culture recommended by American type culture collection (ATCC), see Supplementary data Table 1. All the mediums were supplemented with 10% fetal bovine serum (FBS) and 1% penicillin/streptomycin. Cultures were maintained at 37 °C in a CO_2 incubator with a controlled humidified atmosphere composed of 95% air and 5% CO_2.

5.2.3. In vitro enzyme assays

The enzyme inhibition activity of CHEQ-1~CHEQ-6 was measured according to the method reported previously. Briefly, 10 μL of enzyme (300 ng of CDC25A or 200 ng of CDC25B) was preincubated for 20 min with the different concentrations of compounds or with DMSO, as a vehicle control. The reaction mixture including 5 μL of reaction buffer (100 mM Tris–HCl, pH 8.2, 40 mM NaCl, 1 mM DTT, and 20% glycerol) and 10 μL of substrate assay solution (0.5 mM OMFP, 3-O-methylfluorescein phosphate) were added to initiate the reaction. The reaction was performed in a water bath at 37 °C for 30 min. Then 100 μL of BIOMOL Green Reagent (BioMol, USA) were added and the samples were incubated at room temperature for 30 min to allow development of the green color. The absorbance of the reaction solution was measured in a spectrophotometer at 630 nm by a microplate reader. IC_{50} values were then estimated at least three times and the averaged values were selected.

5.2.4. Cell viability assay

The effect of CHEQ-1~CHEQ-6 on cellular viability was assessed by using the MTT assay. Cells were seeded at an initial density of 3000 cells per well in 96-well culture plates (Costar, USA) 24 h prior

to the experiment. Then the cells were treated with various concentrations of XDW-1, VK3 or CHEQ-1~CHEQ-6 for 48 h. At the end of the time point, MTT was added to the medium (0.5 mg/mL) and incubated at 37 °C for 4 h. The resulting insoluble formazan was dissolved with DMSO and measured at 570 nm using a spectrophotometer. IC_{50} values were then estimated at least three times and the averaged values were selected.

5.2.5. Cell cycle analysis

The ratio of HT29, HepG2 and MCF-7 cells in the G0/G1, S and G2/M phases of cell cycle was determined by their DNA content. Cells were treated with or without various concentrations of CHEQ-2 for 48 h and then harvested, washed twice with cold PBS, and fixed with 75% ice-cold ethanol overnight. Fixed cells were washed twice with cold PBS and incubated with 5 μL of 100 μg/mL RNase A for 30 min at 37 °C. After incubation, the cells were stained with 50 μg/mL PI for 15 min in the dark room and analyzed by flow cytometry. Untreated cells were used as a control.

5.2.6. ROS production assay

Intracellular ROS levels were analyzed using the ROS-sensitive dye, 2′,7′-Dichlorofluorescin diacetate (DCFH-DA, Sigma, USA). DCFH-DA is a cell-permeable non-fluorescent probe, which can be de-esterified intracellularly and turned into highly fluorescent 2′,7′-dichlorofluorescein (DCF) upon oxidation. DCFH-DA dissolved in absolute ethanol (10 mM), was used at a final concentration of 10 μM. Cells were treated with or without various concentrations of CHEQ-2 for 48 h until culture medium was replaced with serum-free medium. ROS probes were then added and incubated for 30 min at 37 °C. The cells were harvested for image capture by fluorescence microscope or flow cytometry analysis.

5.2.7. Mitochondrial membrane potential ($\Delta\psi$) assay

Mitochondrial membrane potential was determined using the Beyotime Mitochondrial Membrane Sensor kit (Beyotime, China) by measuring the potential-dependent accumulation of 5,5′,6,6′-tetrachloro-1,1′,3,3′tetraethylbenzimidazolylcarbocyanine iodide (JC-1). JC-1 aggregates in the mitochondria of healthy cells and emits red fluorescence against a green monomeric cytoplasmic background staining. However, in cells with a collapsed mitochondrial membrane potential, the dye is not able to accumulate in the mitochondria and remains as monomers throughout the cells emitting green fluorescence [15]. After 48 h of CHEQ-2 treatment, cells were washed with PBS once, then incubated with JC-1 staining solution according to the manufacturer's specification for 20 min at 37 °C. After staining, the cells were harvested for image capture by fluorescence microscope or flow cytometry analysis.

5.2.8. Hoechst 33342 staining

Fluorescent dye Hoechst 33342 was used to observe the Chromatin condensation of the cells. HT-29, HepG2 and MCF-7 cells were seeded into 6-well plate 24 h prior to the experiment. The cells were then treated with different concentrations of CHEQ-2 for the next 48 h. The cells were washed with PBS once and incubated with 2 μg/mL Hoechst 33342 at 37 °C for 30 min. Chromatin condensation was observed by fluorescence microscopy.

5.2.9. Annexin V–FITC/PI staining experiment

Apoptosis was assessed by annexin V–fluorescence isothiocyanate (FITC)/PI apoptosis detection kit (Beyotime, China). The externalization of phosphatidylserine, an early apoptotic event, was analyzed by flow cytometry-based annexin V binding assays after treatment with different concentrations of CHEQ-2 for 48 h. After treatment, cells were digested and washed twice with PBS. The cells were re-suspended in 200 μL of binding buffer, stained with Annexin V–FITC (20 μg/mL) and 5 μL of propidium iodide (PI, 50 μg/mL) for 30 min in the dark room, and then diluted with an additional 300 μL of binding buffer. The apoptotic index was determined by flow cytometry (BD FACScan™, USA), and the form scatter diagram was analyzed.

5.2.10. Western blot analysis

Western blot analysis was performed as described previously [32]. Briefly, total protein from the cells was extracted in RIPA lysis buffer (Beyotime, China) supplemented with protease inhibitor cocktail tablets (complete ULTRA Tablets, Roche) and quantified using a BCA Protein Assay Kit (Thermo Fisher Scientific, USA). A total of 30 μg of protein was separated using 10% SDS-PAGE and electrophoretically transferred to a PVDF membrane (Millipore, USA). The membrane was blocked with 5% nonfat milk and incubated at 4 °C overnight with the desired primary antibody. After washing three times with PBS containing 0.05% Tween-20 (PBST), the membrane was incubated for 70 min with horseradish peroxidase-conjugated secondary antibody diluted in PBST. Protein bands were visualized using enhanced chemiluminescence (Millipore, USA) and detected using a ChemiDoc XRS + Imaging System (Bio-rad, USA).

5.2.11. Acute toxicity experiment

Mortality and clinical signs were continually observed for 0, 1, 2, 3, 4, 5, and 6 h after oral administration or abdominal injection of a single dose (2000 mg/kg) on day 0 and at one time per day from day 1 to day 14. The animals (10 mice per group) were weighed before dosing (day 0, justified as 100%) and after dosing (day 1 to day 7, once a day) using an electronic balance (Sartorius Co., Germany). After 7 days, the body weights of animals were no longer recorded and clinical signs were continued observed. On day 14, all animals were euthanized by cervical vertebra luxation and examined for internal organ abnormalities.

5.2.12. Tumor xenograft experiment

All nude mice were housed in sterile cages within laminar air flow hoods under specific pathogen-free conditions with sterile food and water ad libitum. Exponentially growing HepG2 cells were harvested, washed with PBS, and resuspended at a concentration of 1×10^7/mL. The left flank of mice was sterilized with iodophor and then inoculated subcutaneously with 0.1 mL of cell suspension (approximately 1×10^6 cells). Tumor development was followed by caliper measurements in 2 dimensions (L and W), and the volume (V) of the tumor was calculated by the formula for a prolate ellipsoid ($V = L \times W^2 \times 3.14/6$) as reported [33]. The treatment started when the average volume of tumor reached 150 mm^2. For treatment with CHEQ-2, the mice were given 10 mg/kg of CHEQ-2 daily by oral administration, while the control mice received vehicle solvent. After 14 days of treatment, the animals were euthanized. And the tumors were harvested, weighed, and prepared for further examination. All animal experiments were performed according to a protocol approved by the Institutional Animal Care and Use Committee.

5.2.13. Statistical analysis

Data are expressed as the means ± S.D. Statistical comparisons were performed by two-way ANOVA followed by Fisher's protected least significance difference (PLSD) test. A probability value <0.05 was considered statistically significant.

Acknowledgments

The financial support from the National Natural Science Foundation of China (NSFC No. 81102320), Research Fund for the Doctoral Program of Higher Education of China (No.

20110131120037), Independent Innovation Foundation of Shandong University (IIFSDU, No. 2010GN044), Shandong Postdoctoral Innovation Science Research Special Program (No. 201002023), and China Postdoctoral Science Foundation funded project (Nos. 20100481282, 2012T50584) is gratefully acknowledged.

The authors have declared no conflict of interest.

Appendix A. Supplementary data

Supplementary data related to this article can be found at http://dx.doi.org/10.1016/j.ejmech.2014.05.063.

References

[1] C.J. Sherr, Cancer cell cycles, Science 74 (1996) 1672–1677.
[2] G. Evan, K.H. Vousden, Proliferation, cell cycle and apoptosis in cancer, Nature 411 (2001) 342–348.
[3] C. Golias, A. Charalabopoulos, K. Charalabopoulos, Cell proliferation and cell cycle control: a mini review, Int. J. Clin. Pract. 58 (2004) 134–141.
[4] K. Vermeulen, D. Van Bockstaele, Z. Berneman, The cell cycle: a review of regulation, deregulation and therapeutic targets in cancer, Cell Prolif. 36 (2003) 131–149.
[5] M. Park, S. Lee, Cell cycle and cancer, J. Biochem. Mol. Biol. 36 (2003) 60–65.
[6] M. Malumbres, M. Barbacid, To cycle or not to cycle: a critical decision in cancer, Nat. Rev. Cancer 1 (2001) 222–231.
[7] C. Karlsson-Rosentha, J. Millar, Cdc25: mechanisms of checkpoint inhibition and recovery, Trends Cell Biol. 16 (2006) 285–292.
[8] A. Lindqvist, H. Källström, A. Lundgren, E. Barsoum, C.K. Rosenthal, Cdc25B cooperates with Cdc25A to induce mitosis but has a unique role in activating cyclin B1-Cdk1 at the centrosome, J. Cell Biol. 171 (2005) 35–45.
[9] B.G. Gabrielli, C.P. De Souza, I.D. Tonks, J.M. Clark, N.K. Hayward, K.A. Ellem, Cytoplasmic accumulation of CDC25B phosphatase in mitosis triggers centrosomal microtubule nucleation in HeLa cells, J. Cell Sci. 109 (1996) 1081–1093.
[10] C.P. De Souza, K.A. Ellem, B.G. Gabrielli, Centrosomal and cytoplasmic Cdk2/cyclin B1 activation precedes nuclear mitotic events, Exp. Cell Res. 257 (2000) 11–21.
[11] B.G. Gabrielli, J.M. Clark, A.K. McCormack, K.A. Ellem, Hyperphosphorylation of the N-terminal domain of cdc25 regulates activity toward cyclinB1/cdc2 but not cyclin A/cdk2, J. Biol. Chem. 272 (1997) 28607–28614.
[12] M.O. Contour-Galcéra, O. Lavergne, M.C. Brezak, B. Ducommun, G. Prévost, Synthesis of small molecule CDC25 phosphatases inhibitors, Bioorg. Med. Chem. Lett. 14 (2004) 5809–5812.
[13] S.W. Ham, H.J. Park, D.H. Lim, Studies on menadione as an inhibitor of the cdc25 phosphatase, Bioorg. Chem. 25 (1997) 33–36.
[14] H. Park, Y.J. Bahn, S.K. Jung, D.G. Jeong, S.H. Lee, I. Seo, T.S. Yoon, S.J. Kim, S.E. Ryu, Discovery of novel Cdc25 phosphatase inhibitors with micromolar activity based on the structure-based virtual screening, J. Med. Chem. 51 (2008) 5533–5541.
[15] N. Delaet, N. Ohmawari, H. Nakai, Preparation of 4,5-Diaryl-1,2,4-triazole-3-thiones and Analogs as Sphingomyelinase Inhibitors. From PCT Int. Appl., WO 2002066447 A1 20020829, 2002.
[16] X. Li, P. Zhan, H. Liu, D. Li, L. Wang, X. Chen, H. Liu, C. Pannecouque, J. Balzarini, E. De Clercq, X. Liu, Arylazolyl(azinyl)thioacetanilides. Part 10: design, synthesis and biological evaluation of novel substituted imidazopyridinylthioacetanilides as potent HIV-1 inhibitors, Bioorg. Med. Chem. 20 (2012) 5527–5536.
[17] R. Boutros, V. Lobjois, B. Ducommun, CDC25 phosphatases in cancer cells: key players? Good targets? Nat. Rev. Cancer 7 (2007) 495–507.
[18] I. Blomberg, I. Hoffmann, Ectopic expression of Cdc25A accelerates the G(1)/S transition and leads to premature activation of cyclin E- and cyclin A-dependent kinases, Mol. Cell. Biol. 19 (1999) 6183–6194.
[19] I. Hoffmann, G. Draetta, E. Karsenti, Activation of the phosphatase activity of human cdc25A by a cdk2-cyclin E dependent phosphorylation at the G1/S transition, EMBO J. 13 (1994) 4302–4310.
[20] S. Jinno, K. Suto, A. Nagata, M. Igarashi, Y. Kanaoka, H. Nojima, H. Okayama, Cdc25A is a novel phosphatase functioning early in the cell cycle, EMBO J. 13 (1994) 1549–1556.
[21] M. Molinari, C. Mercurio, J. Dominguez, F. Goubin, G.F. Draetta, Human Cdc25 A inactivation in response to S phase inhibition and its role in preventing premature mitosis, EMBO Rep. 1 (2000) 71–79.
[22] H. Zhao, J.L. Watkins, H. Piwnica-Worms, Disruption of the checkpoint kinase 1/cell division cycle 25A pathway abrogates ionizing radiation-induced S and G2 checkpoints, Proc. Natl. Acad. Sci. U. S. A. 99 (2002) 14795–14800.
[23] G.K. Schwartz, M.A. Shah, Targeting the cell cycle: a new approach to cancer therapy, J. Clin. Oncol. 23 (2005) 9408–9421.
[24] D. Sampath, Z. Shi, W. Plunkett, Inhibition of cyclin-dependent kinase 2 by the Chk1-Cdc25A pathway during the S-phase checkpoint activated by fludarabine: dysregulation by 7-hydroxystaurosporine, Mol. Pharmacol. 62 (2002) 680–688.
[25] J.E. Chipuk, D.R. Green, How do BCL-2 proteins induce mitochondrial outer membrane permeabilization? Trends Cell Biol. 18 (2008) 157–164.
[26] L. Lalier, P.F. Cartron, P. Juin, S. Nedelkina, S. Manon, B. Bechinger, F.M. Vallette, Bax activation and mitochondrial insertion during apoptosis, Apoptosis 12 (2007) 887–896.
[27] L. Scorrano, S.J. Korsmeyer, Mechanisms of cytochrome c release by proapoptotic BCL-2 family members, Biochem Biophys. Res. Commun. 304 (2003) 437–444.
[28] V. Petronilli, G. Miotto, M. Canton, R. Colonna, P. Bernardi, F. Di Lisa, Review imaging the mitochondrial permeability transition pore in intact cells, Biofactors 8 (1998) 263–272.
[29] M. Brisson, C. Foster, P. Wipf, B. Joo, R.J. Tomko Jr., T. Nguyen, J.S. Lazo, Independent mechanistic inhibition of cdc25 phosphatases by a natural product caulibugulone, Mol. Pharmacol. 71 (2007) 184–192.
[30] J. Rudolph, Redox regulation of the Cdc25 phosphatases, Antioxid. Redox Signal 7 (2005) 761–767.
[31] G. Buhrman, B. Parker, J. Sohn, J. Rudolph, C. Mattos, Structural mechanism of oxidative regulation of the phosphatase Cdc25B via an intramolecular disulfide bond, Biochemistry 44 (2005) 5307–5316.
[32] Y. Song, X. Guo, B. Zheng, X. Liu, X. Dong, L. Yu, Y. Cheng, Ligustrazine derivate DLJ14 reduces multidrug resistance of K562/A02 cells by modulating GSTπ activity, Toxicol. In Vitro 25 (2001) 937–943.
[33] J.J. Maoret, Y. Anini, C. Rouyer-Fessard, D. Gully, M. Laburthe, Neurotensin and a non-peptide neurotensin receptor antagonist control human colon cancer cell growth in cell culture and in cells xenografted into nude mice, Int. J. Cancer 80 (1999) 448–454.